Mesenchymal niche-derived Neuregulin 1 drives intestinal stem cell proliferation and regeneration of damaged epithelium

Thierry Jardé[1,2,3,*], Wing Hei Chan[1,2,15], Fernando J. Rossello[1,4,5,15], Tanvir Kaur Kahlon[1,2], Mandy Theocharous[6,7], Teni Kurian Arackal[1,2], Tracey Flores[1,2], Mégane Giraud[1,2], Elizabeth Richards[1,2], Eva Chan[1,2], Genevieve Kerr[1,2], Rebekah M. Engel[1,2,8], Mirsada Prasko[1,2], Jacqueline F. Donoghue[3,9], Shin-ichi Abe[10], Toby J. Phesse[11], Christian M. Nefzger[1,2,4,12], Paul J. McMurrick[8], David R. Powell[13], Roger J. Daly[6,7], Jose M. Polo[1,2,4], Helen E. Abud[1,2,14,*]

[1]Department of Anatomy and Developmental Biology, Monash University, Clayton, Victoria, 3800, Australia

[2]Development and Stem Cells Program, Monash Biomedicine Discovery Institute, Clayton, Victoria, 3800, Australia

[3]Centre for Cancer Research, Hudson Institute of Medical Research, Clayton, Victoria, 3168, Australia

[4]Australian Regenerative Medicine Institute, Monash University, Clayton, Victoria, 3800, Australia

[5]University of Melbourne Centre for Cancer Research, University of Melbourne, Melbourne, Victoria, 3000, Australia

[6]Department of Biochemistry and Molecular Biology, Monash University, Melbourne, Victoria, 3800, Australia

[7]Cancer Program, Monash Biomedicine Discovery Institute, Clayton, Victoria, 3800, Australia

[8]Cabrini Monash University Department of Surgery, Cabrini Hospital, Malvern, Victoria, 3144, Australia

[9]Department of Obstetrics and Gynaecology, Royal Women's Hospital, Melbourne University, Melbourne, Victoria, 3052, Australia.

[10]Center for Education, Kumamoto Health Science University, Kumamoto, 861-5598, Japan.

[11]European Cancer Stem Cell Research Institute, Cardiff University, School of Biosciences, Cardiff, CF24 4HQ, UK and Doherty Institute of Infection and Immunity, University of Melbourne, Melbourne, Victoria 3000, Australia.

[12]Institute for Molecular Bioscience, The University of Queensland, St Lucia, Queensland, 4072, Australia

[13]Monash Bioinformatics Platform, Monash University, Clayton, Victoria, 3800, Australia

[14] Lead Contact

[15] These authors contributed equally to this work

*Correspondance jardethierry@yahoo.fr, helen.abud@monash.edu

Summary

The proliferation of intestinal stem cells is maintained by EGF, a key component of the medium required to support organoids *ex vivo*. Here, we identified that NRG1, not EGF, is up-regulated during tissue repair following injury. NRG1 is expressed in mesenchymal stromal cells, macrophages and Paneth cells. Knockout of NRG1 produced a decrease in cell proliferation within crypts and a reduced capacity to regenerate following injury. Treatment with NRG1 robustly stimulated proliferation in crypts and budding of organoids. Molecular characterisation of the effects of NRG1 revealed an elevated and sustained activation of MAPK and AKT and a proliferative signature. NRG1 also had a strong impact on the expression of stem cell markers, the ability of progenitor cells to initiate organoid growth and enhanced regeneration. Our data suggest mesenchymal-derived NRG1 is a potent mediator of tissue regeneration and may inform the development of NRG1-based therapies for enhancing intestinal repair after injury.

Introduction

Self-renewal and differentiation of intestinal stem cells (ISCs) within crypts are coordinated by key niche signals secreted from supporting pericryptal mesenchymal cells, macrophages and Paneth cells (Degirmenci et al., 2018b; Farin et al., 2012; McCarthy et al., 2020; Sato et al., 2011; Shoshkes-Carmel et al., 2018; Valenta et al., 2016). The interplay between different signalling pathways determines the balance between expansion and survival of stem/progenitor cells and cell fate commitment to secretory or absorptive differentiation pathways. The core signalling pathways that orchestrate these decisions are the WNT, NOTCH, BMP and epithelial growth factor (EGF) signalling pathways (Clevers, 2013; Farin et al., 2012; Horvay and Abud, 2013; Jarde et al., 2013; Kabiri et al., 2018; McCarthy et al., 2020; Tian et al., 2015). Regulation of signalling is particularly important during the substantial regenerative response triggered upon epithelial injury to ensure adequate tissue repair without aberrant proliferation. During this process, secretory and absorptive progenitor cells de-differentiate into new Lgr5+ ISCs and initiate the extensive cell division program crucial for restoring epithelial integrity (Ayyaz et al., 2019; Buczacki et al., 2013; de Sousa and de Sauvage, 2019; Murata et al., 2020; Nusse et al., 2018; Tetteh et al., 2016; Tian et al., 2011; van Es et al., 2012; Wang et al., 2019; Yui et al., 2018). YAP and IL6/STAT signalling pathways and secreted R-spondin play key roles in the regenerative process (Ayyaz et al., 2019; Gregorieff et al., 2015; Harnack et al., 2019; Taniguchi et al., 2015; Yui et al., 2018). However, the repertoire of signals that drive tissue remodelling and the massive but transient increase in proliferative crypts are unclear.

A major driver of intestinal epithelial cell proliferation is the EGF signalling pathway (Abud et al., 2005; Basak et al., 2017; Biteau and Jasper, 2011; Lee et al., 2008; Pejchal et al., 2015). In mammals, the EGFR/ERBB receptor family comprises four receptor tyrosine kinases EGFR, ERBB2, ERBB3 and ERRB4. These receptors are activated by binding of a family of ligands that include EGF, transforming growth factor α (TGFα), amphiregulin and epigen which interact with EGFR, as well as heparin-binding EGF-like growth factor, epiregulin, betacellulin and Neuregulin (NRG) 1-4 that interact with multiple receptors (Lemmon et al., 2014). Ligand-induced receptor homo or heterodimerisation (Burgess et al., 2003; Schlessinger, 2002) activates signalling cascades such as the mitogen-activated protein kinase (MAPK) pathway and PI3-kinase/AKT signalling (Amit et al., 2007; Grant et al., 2002; Olayioye, 2001).

In the midgut region of the *Drosophila* intestine, EGF signalling is required to maintain the proliferative capacity of ISCs and drive the regenerative response following damage induced by infection (Biteau and Jasper, 2011; Buchon et al., 2010; Jiang et al., 2011). In the

mammalian intestine, EGF is secreted by Paneth and stromal cells and is a key element of the culture conditions required for supporting *ex vivo* intestinal organoid cultures (Sato et al., 2011; Sato et al., 2009). However, mice which lack EGF are viable and fertile. In fact, knockout of EGF alongside two other members of the EGF family of ligands, amphiregulin and TGFα, still results in animals that are healthy and fertile with normal intestinal tissue architecture (Luetteke et al., 1999). This contrasts with receptor knockouts which produce more profound phenotypes, including severe intestinal defects (Erickson et al., 1997; Lee et al., 1995; Miettinen et al., 1995; Threadgill et al., 1995). However, knockout of EGFR on some genetic backgrounds are viable (Sibilia and Wagner, 1995) and single knockout of EGFR and ERBB3 in the intestinal epithelium are well tolerated, suggesting some redundancy of receptor function (Lee et al., 2009; Srivatsa et al., 2017). The phenotypic differences observed between ligand and receptor knockouts overall, suggests other ligands that interact with EGFR family must be responsible for driving ISC proliferation.

The NRGs, which are part of the EGF family of ligands, interact with EGF and ERBB receptors (Britsch, 2007). NRG1 is critical for the establishment and proliferation of mouse mammary gland organoids (Jarde et al., 2016). Furthermore, NRG1 has been implicated as a key driver of regeneration in a variety of tissues. For example, NRG1 secreted from nerves drives proliferation of cells within the blastema during regeneration of axolotl limbs (Farkas et al., 2016) and regulates repair mechanisms of spinal axons after injury (Bartus et al., 2016). NRG1 is also induced during cardiac damage in zebrafish (Gemberling et al., 2015) and can induce proliferation of cardiomyocytes (Rupert and Coulombe, 2015). However, the regenerative properties of this ligand in the intestine *in vivo* have not yet been explored.

In this study, we investigated the role of EGF ligands during the regeneration of the epithelium following damage. Surprisingly, we found that NRG1, not EGF, is up-regulated by niche cells during tissue regeneration. Our data also revealed robust induction of proliferation of ISCs and progenitors by NRG1, which challenges the concept that EGF is the main signalling ligand that drives proliferation of intestinal cells. This data provides critical insight into the regenerative signals activated upon damage and supports a model where NRG1 is up-regulated following injury in mesenchymal cells to drive proliferation in crypts.

Results

NRG1 is induced during the regenerative response following intestinal injury

To investigate the role of EGF family ligands in epithelial repair following tissue damage, we challenged wild-type mice using two injury models, 13 Gy irradiation and exposure to 5-fluorouracil (5-FU). Both models induce DNA damage and apoptosis in proliferative cells within intestinal crypts (Potten and Grant, 1998). This results in a dramatic shortening of crypts at day 2, followed by a period of rapid regeneration where progenitor cells display extensive plasticity and de-differentiate to drive increased proliferation, leading to crypt cell repopulation (Figures S1A and S1B) (Ayyaz et al., 2019; Horvay et al., 2015; Murata et al., 2020; Nusse et al., 2018; Wang et al., 2019; Yui et al., 2018).

The expression of EGF and NRG ligands during tissue regeneration was quantified in the small intestine (SI) following damage after injury (day 2 post-treatment) and during regeneration (day 5 post-injury) (Figures 1A, 1C, S1C, and S1D). Alongside this, the expression of ISC markers *Lgr5* and *Olfm4* were examined. Two days after injury, *Olfm4* and *Lgr5* expression was down-regulated as a reflection of injury-induced stem cell loss, but were restored by day 5 (Figures 1A, 1C, S1A and S1B) (Nusse et al., 2018; Yui et al., 2018). Strikingly, regeneration was marked by a robust increase in *Nrg1* expression in both injury models, in contrast to the other ligands, where expression was either down-regulated or unaltered (Figures 1A, 1C, S1C and S1D). A strong NRG1 signal was detected in the vicinity of regenerating crypts post injury (Figure 1B and 1D). The expression of the NRG1 receptor, ERBB3, was more abundant in regenerating crypts in both injury models (Figure S1E and S1F). These data suggest that NRG1 is a key endogenous ligand contributing to intestinal tissue regeneration following damage.

NRG1 can substitute for EGF and promote robust proliferation of intestinal organoids

To investigate the capacity of NRG1 to sustain efficient regeneration, proliferation and differentiation, we examined the ability of NRG1 to support the growth of SI organoids. Organoid culture can also be considered a regeneration model as it involves activation of defined signalling pathways critical for tissue regeneration, including transient activation of YAP, and leads to the development of complex intestinal structures starting from a single isolated crypt (Chiacchiera et al., 2016; Date and Sato, 2015; Sato et al., 2009; Serra et al., 2019). In the presence of EGF, which is one of the original constituents of the growth factor cocktail (Sato et al., 2009), organoids developed crypt domains that contain BrdU+ proliferative cells. In marked contrast, organoids treated with NRG1 and without EGF were

much larger, with buds comprised of numerous rapidly proliferating cells, as shown by BrdU incorporation (Figures 1E and 1F). NRG1 dramatically increased organoid growth by 4-fold compared to EGF over 4 days (Figure 1G). EGF was no longer required, demonstrating that NRG1 can substitute for EGF. Furthermore, no cumulative effect was evident when both EGF and NRG1 were present (Figure 1G).

The activation of MAPK and PI3K-AKT signalling downstream of NRG1 has been described in several contexts (Britsch, 2007). To determine whether these signalling pathways were activated during the strong proliferative response induced by NRG1, fully-formed organoids established in ENR (EGF, Noggin, R-spondin 1) medium were starved of EGF for 5 hours, then exposed to EGF or NRG1. More robust activation of both the MAPK and AKT pathways by NRG1 was evident compared to EGF, quantified by the level of phosphorylated ERK and AKT following 15 minutes of stimulation. This activation was maintained for at least 5 hours (Figure 1H). We also tested whether NRG1 was able to activate these signalling pathways in complete medium, which contains EGF. Following 1 hour of treatment with NRG1, phosphorylation of AKT and ERK was robustly increased in organoids compared to EGF treatment alone (Figure S1G). This correlation between NRG1 stimulation and strong activation of MAPK and PI3K-AKT signalling may underlie the strong proliferative response mediated by NRG1 and this effect can be induced in the presence of EGF ligand.

The ability of NRG1 and EGF to trigger the phosphorylation of ERBB2 and ERBB3 receptors was examined in organoids. NRG1 was more potent than EGF in inducing phosphorylation of both ERBB2 and ERBB3 (Figure S1H and S1I). We then assessed the functional contribution of EGF receptor ERBB1 in mediating NRG1-induced organoid growth. Intestinal organoids cultured with EGF and the ERBB1 inhibitor gefitinib failed to form buds (Figure S1J). In contrast, organoids cultured with both NRG1 and gefitinib contained budding crypt domains and KI-67 proliferative cells (Figure S1J). Importantly, treatment of organoids with NRG1 in the presence of gefitinib maintained organoid growth as the total number of cells was similar between cultures treated with EGF alone and NRG1 combined with gefitinib (Figure S1K).

Taken together, these data suggest that the up-regulation of NRG1 observed following damage supports the proliferative regenerative response, which is underpinned by the ability of NRG1 to robustly activate ERBB2 and ERBB3 receptors and downstream AKT and ERK signalling.

NRG1 is secreted by mesenchymal and epithelial niche cells

To identify the cellular source of NRG1, SI mesenchymal populations were purified from control mice and compared to tissue undergoing regeneration following damage, using cell surface markers (Figure S2). Live single cells were stratified into CD45+ F4/80+ CD11b+ (macrophage-enriched), CD45+ F4/80- CD11b- (leukocytes without macrophages), CD45- CD31+ (endothelial cells), CD45- CD31- GP38- cells and CD45- CD31- GP38+ CD34+/- PDGFRα+/- (stromal) cells (Figure S2A). Both macrophages and CD34+/- PDGFRα+ stromal populations have been described as key niche components due to their role in maintaining ISC function and/or secreting WNT and BMP signalling molecules (Greicius et al., 2018; McCarthy et al., 2020; Sehgal et al., 2018; Shoshkes-Carmel et al., 2018; Stzepourginski et al., 2017). We confirmed the purity of the sorted cell populations by assessing the expression of key marker genes (Figure S2B). During tissue homeostasis, *Nrg1* was strongly expressed in CD34- PDGFRα+ and CD34- PDGFRα- stromal cells, macrophages and endothelial cells (Figure 2A). Strikingly, following both radiation and 5-FU-induced injury, *Nrg1* expression was strongly elevated in macrophages (4.8-fold and 8.3-fold) and CD34- PDGFRα+ stromal cells (13.8-fold and 4.5-fold) compared to homeostatic conditions (Figure 2A). Furthermore, in CD34+ PDGFRα+ stromal cells, where *Nrg1* is barely detectable under steady state conditions, *Nrg1* was highly elevated following radiation-induced damage (Figure 2A). No changes in *Egf* were detected in these cell populations in either injury model (Figure 2C). Only minor changes in the relative proportion of different cell types were noted for the irradiation model (Figure S2C). We confirmed the expression of NRG1 in distinct cell populations by co-immunofluorescence (Figure 2B). NRG1 partially over-lapped with F4/80+ and PDFGRα+ cells that were found in the close vicinity of regenerating crypts, confirming expression of NRG1 in a sub-set of these cells. There was no co-localisation of NRG1 and alpha smooth muscle actin (αSMA) (Figure S3A).

The expression of NRG1 was also examined in epithelial cells. Utilising tissue isolated from Lgr5-EGFP transgenic mice, which allows detection of ISCs by reference to GFP, we observed that NRG1 was expressed by a population of epithelial cells located at the bottom of the crypts adjacent but distinct from the crypt base columnar (CBC) cells (Figure 2D). Co-immunostaining confirmed that NRG1 was expressed by Lysozyme-positive Paneth cells, which are known to provide niche signals, including EGF (Figure S3B) (Sato et al., 2011). No obvious changes in NRG1 staining intensity were observed in Paneth cells at day 5 post-13 Gy irradiation (Figure S3C).

The expression of ERBB3 was rarely observed in mesenchymal cells, but was detected in basolateral membranes of epithelial cells, including Lgr5+ stem cells (Figure 2D). To further explore these findings, we isolated Lgr5-GFP^{high} stem cells, their daughter cells (Lgr5-GFP^{med} and Lgr5-GFP^{low}) and a CD24^{high} Paneth cell-enriched population by FACS. After validating the identity of these populations (Figure S3D), we examined the expression of *Nrg1* and *ErbB* receptors. *Nrg1* levels were 26-fold higher in Paneth cells compared to stem cells (Figure S3D), confirming our observations by immunofluorescence. *ErbB2* and *ErbB3* levels were also higher in stem cells compared to Paneth cells (Figure S3D). *Nrg1* expression was significantly higher in mesenchyme compared to epithelium (Figure S3E and S3F), while *ErbB2* and *ErbB3* receptors were most highly expressed in the epithelium (Figure S3F). These results suggest a paracrine signalling network operates during tissue homeostasis and tissue regeneration, whereby supporting mesenchymal cells and Paneth cells secrete NRG1, which acts on the epithelium, including stem and progenitor transit amplifying cells, via ERBB3/ERBB2 receptors.

Nrg1 supports intestinal stem cell maintenance and proliferation during regeneration

The requirement for NRG1 during intestinal homeostasis was investigated by conditional deletion of *Nrg1* in SI tissue of adult mice. The specific function of *Nrg1* in distinct intestinal cell compartments (Paneth cells vs mesenchymal cells) was explored using different Cre drivers. Villin-Cre-ER^{T2} (el Marjou et al., 2004) was utilised to drive expression of Cre recombinase specifically in the epithelium and the global inducible Ubc-Cre-ER^{T2} (Ruzankina et al., 2007) was used to produce knockout in all the different cell populations that express *Nrg1* in the mesenchyme and epithelium. These Cre drivers were crossed with *Nrg1*$^{fl/fl}$ mice, which contain loxP sites flanking exon 6 of the *Nrg1* gene that encodes for the active EGF-like domain (Zhang et al., 2011). Following induction of Cre recombinase with tamoxifen, tissues from Villin-Cre-ER^{T2} *Nrg1*$^{+/+}$ control and Villin-Cre-ER^{T2} *Nrg1*$^{fl/fl}$ test mice were collected on day 5 and day 16 (Figure S4A and S4E). Knockout of epithelial *Nrg1* was confirmed and revealed a significant reduction (81%) in Nrg1 expression (Figure S4D). However, despite extensive analyses, no overt morphological, histological or proliferative differences could be detected in *Nrg1* epithelial-specific knockout mice at either day 5 (Figure S4B-S4D) or 16 (Figure S4F-S4H). To assess whether mesenchymal cells were compensating for epithelial loss of *Nrg1*, we established SI organoid cultures from both Villin-Cre-ER^{T2} *Nrg1*$^{+/+}$ and Villin-Cre-ER^{T2} *Nrg1*$^{fl/fl}$ mice. Following tamoxifen treatment in culture and subsequent knockout of *Nrg1* (Figure S4I), there was no difference in overall organoid morphology and growth in

knockout organoids grown in ENR medium (Figure S4J and S4K), suggesting EGF in the medium could support organoid growth in the absence of NRG1.

We then explored whether concomitant loss of *Nrg1* in both epithelial and mesenchymal compartments could impact intestinal tissue homoeostasis. We utilised the Ubc-Cre-ER^{T2} inducible Cre driver and first evaluated the efficiency of this allele in driving recombination using the ROSA26-ZsGreen1 reporter system (Figure S5A) (Madisen et al., 2010). Eight days following tamoxifen injection, ZsGreen1 expression was observed in both epithelial and mesenchymal compartments, including pericryptal cells and the muscularis mucosa (Figure S5B) which validated the use of the Ubc-Cre-ER^{T2} model. Following Cre-induction, intestinal tissues were collected at day 16 (Figure 3A) as previous studies suggest this time frame is sufficient to delete secreted signalling molecules in niche cells (McCarthy et al., 2020; Valenta et al., 2016). Loss of *Nrg1* (Figure 3B) produced clear morphological changes in the epithelium, including a 20% reduction in the size of the crypt and villus compartments (Figure S5C) and a significant decrease in the number of BrdU+ proliferative crypt cells and BrdU+ CBC stem cells in mutant tissues compared to controls (Figure 3C and 3D). There were no changes in differentiated goblet, Paneth and enteroendocrine cells (Figure S5D). Importantly, the *Olfm4*+ stem cell pool was impacted by the loss of *Nrg1*, as indicated by a 25% decrease in the number of *Olfm4*+ cells in mutant crypts (Figure 3E). Interestingly, knockout of *Nrg1* expression was not maintained at day 31 post-tamoxifen treatment, suggesting a selective pressure for repopulation of intestinal mesenchymal tissues by unrecombined cells, although a significant decrease in OLFM4+ cells were still observed at this time-point (Figure S5E-5I).

We next explored the requirement for *Nrg1* during intestinal regeneration following damage. Following knockout of *Nrg1,* mice were exposed to 13 Gy irradiation to induce tissue damage and subsequent regeneration (Figure 3F). At day 5 post-treatment, loss of *Nrg1* significantly impaired the regenerative capacity of the intestinal tissue as marked by a decrease in the number of regenerating crypts and strong reduction in the number of BrdU+ (-41%) and OLFM4+ (-39%) cells per crypt in knockout mice compared to controls (Figure 3G-3J). Moreover, similar profound intestinal alterations were observed in *Nrg1* knockout mice at day 4 post-injury using the 5-FU model (Figure 3K-3O). This could be due to either depletion of the pool of cells required for the initiation of the regenerative response or an impact on the regenerative response.

These functional studies show that endogenous NRG1 is required to sustain cellular proliferation and stem cell maintenance in intestinal crypts during tissue homeostasis and regeneration following damage.

NRG1 promotes cell proliferation and alters differentiation of the stem cell pool

In order to mimic the endogenous up-regulation of NRG1 during regeneration and explore the impact of this on the epithelium, we treated adult C57BL/6 wild-type mice with recombinant NRG1. Mice were treated with intraperitoneal injections of recombinant NRG1 (15 µg/day) or PBS (control) for 5 days (n=8) and tissues were collected on day 6 (Figure 4A). An earlier time point of analysis was selected compared to the *Nrg1* knockout experiment as the NRG1 recombinant protein was directly injected into the mice and did not rely on tamoxifen-mediated loss of *Nrg1* gene and disappearance of the protein from the system. NRG1-treated mice did not display any physical or behavioural symptoms but exhibited a pronounced intestinal phenotype that was characterised by a significant enlargement of the crypt and villus compartments (+22% and +19% respectively) (Figure 4B). The proportion of differentiated secretory cells was also altered, with an increase in goblet cells (Figure S6A) and a decrease in Paneth cells (Figure S6B). In addition, the number of BrdU+ proliferative cells were significantly increased in NRG1-treated mice (Figure 4C). To evaluate whether the stem cell pool was affected by elevated levels of NRG1, the expression of ISC markers, including *EphB2*, *Hes-1*, *Lgr5*, *Olfm4* and *Smoc2*, was assessed. All of these ISC markers were up-regulated in NRG1-treated epithelium (Figure 4D).

Overall, this data demonstrates that elevation of NRG1 drives enlargement of crypts containing proliferative cells and elevation of stem cell marker expression, a phenotype that is opposite to the changes observed after endogenous deletion of *Nrg1*.

NRG1 drives proliferative and stem cell molecular signatures and augments intestinal stem cell function

To characterise the underlying molecular mechanisms responsible for the NRG1-mediated intestinal changes, stem cells ($Lgr5^{high}$-$CD24^{low}$), their immediate progenitors ($Lgr5^{med}$-$CD24^{low}$), subsequent progenitors ($Lgr5^{low}$-$CD24^{low}$) and differentiated cells (double negative) were isolated from NRG1-treated and control Lgr5-EGFP mice (Figure 4E and S6C). We used the CD24 cell surface marker that labels stem and proliferative cells within crypts to isolate a CD24- Lgr5- population without contaminating unlabelled Lgr5+ cells (Nefzger et al., 2016). This population represents a subset of the differentiated cell pool as it excludes both $CD24^{high}$

Paneth and enteroendocrine cells (Sato et al., 2011). Following RNA sequencing, we first evaluated the expression of known stem cell and differentiation markers to validate our sorting strategy (Figure S6D). We then analysed changes mediated by NRG1 in these distinct cell pools (Figure 4F). This revealed that Lgr5^{med}-CD24^{low} and Lgr5^{high}-CD24^{low} cells significantly responded to NRG1 as the number of differentially expressed genes (DEG) (FDR<0.05) was 1308 and 723 respectively, in NRG1-treated cells compared to controls (Figure 4G). In contrast, only around 170 transcripts were differentially expressed in Lgr5^{low}-CD24^{low} and double negative cell populations (Figure 4G). Of note, this lack of response could partially be due to the fact that among the 4 cell populations studied, the Lgr5^{low}-CD24^{low} and double negative cells are the most heterogeneous in nature.

In an effort to understand why intestinal cell populations respond differently to NRG1 stimulation, we compared the molecular signature of untreated Lgr5^{med}-CD24^{low} and Lgr5^{low}-CD24^{low} cells. These two cell populations express similar levels of the receptors *Erbb2* and *Erbb3* and most of the known downstream signalling molecules (Figure S6E), which suggests these two populations have similar abilities to respond to NRG1. Gene ontology analysis was used to determine biological processes that characterise these two cell populations. Analysis of DEG between Lgr5^{med}-CD24^{low} cells and Lgr5^{low}-CD24^{low} cells (781 up-regulated genes in the Lgr5^{low}-CD24^{low} and 466 up-regulated genes in the Lgr5^{med}-CD24^{low} cells, FDR<0.05) showed these two populations were distinct. Lgr5^{low}-CD24^{low} cells appeared to be more advanced on the path to differentiation, exhibiting functions related to digestion of fat and metabolism of lipids (Figure S6F and S6H). In contrast, the gene signature of Lgr5^{med}-CD24^{low} cells was enriched for proliferative cellular functions, including DNA replication., mitotic cell cycle and cell division (Figure S6G and S6H). Importantly, the WNT signalling pathway was also identified, which raises the question of whether active WNT signalling is required for cells respond to NRG1. To test this hypothesis, SI organoids were cultured in the presence of the WNT inhibitor IWP2 or in the absence of R-spondin 1 and supplemented with EGF or NRG1 (Figures 4H, 4I and S6I). Inhibition of WNT signalling resulted in a dramatic decrease in the formation of mature budding organoids that could not be rescued in the presence of NRG1 or EGF. We also tested whether other signalling pathways were required. NRG1 treatment was able to rescue the formation of budding organoids in the presence of both the NOTCH signalling inhibitor DAPT, or the YAP signalling inhibitor verteporfin (Figure 4H and 4I), although there was some impact on overall growth. This data suggests that the effects of NRG1 require the presence of active WNT signalling, which may explain why NRG1 differentially

effects stem and immediate progenitor cells. However, there may also be other mechanisms that contribute to the responsiveness of cells.

Analysis of differentially expressed genes in Lgr5^{med}-CD24^{low} and Lgr5^{high}-CD24^{low} populations revealed that NRG1-regulated genes were associated with mitotic cell cycle processes (Figure 5A). This was not observed in Lgr5^{low}-CD24^{low} and double negative cells. This concurs with our observation of an increased number of BrdU+ cells in intestinal crypts of NRG1-treated mice (Figure 3C and 3D). To demonstrate that NRG1 regulates stem cell proliferation, we performed co-immunofluorescence to detect both Lgr5-GFP CBC cells and BrdU+ cells. The percentage of BrdU+ Lgr5-GFP+ cells was increased 2.1-fold in NRG1-treated mice (Figure 5B). An increase in proliferative progenitor cells was also evident. Single cell PCR analysis of cell cycle-related genes (*Aspm, Ccnb1, Foxm1 and Ki67*) in NRG1-treated Lgr5^{high}-CD24^{low} stem cells also revealed a significant and homogeneous activation of these genes (Figure 5C).

Multidimensional Scaling analysis was utilised to visualise the effect of NRG1 on different intestinal subpopulations. Both Principal Component Analysis (PCA) dimension 1 and dimension 2 allowed identification of a hierarchical stream among populations, going from Lgr5^{high}-CD24^{low} stem cells to the more differentiated cells, Lgr5^{med}-CD24^{low} and then Lgr5^{low}-CD24^{low} (Figures 6A and S7A). Importantly, NRG1-treated cells shifted away from their initial cell identity towards a more undifferentiated state (Figure 6A and S7A). Hierarchical clustering analysis of the entire transcriptome revealed intestinal sub-populations clustered on their cellular identity in a NRG1-independent manner (Figure S7B). However, when we assessed genes specifically regulated by NRG1 in Lgr5^{med}-CD24^{low} cells, these cells clustered with Lgr5^{high}-CD24^{low} stem cells (Figure 6B, S7C and S7D), which indicates NRG1 modulates genes in the Lgr5^{med}-CD24^{low} population to make them more stem cell-like. We identified 584 genes (FDR<0.05) that were expressed at >2 fold higher levels in both NRG1-treated Lgr5^{med}-CD24^{low} cells and untreated Lgr5^{high}-CD24^{low} stem cells compared to untreated Lgr5^{med}-CD24^{low} cells, including numerous stem cell markers (Figure 6C). A similar phenotype was observed for NRG1-treated Lgr5^{high}-CD24^{low} stem cells (Figure 6C). Gene set enrichment analysis was conducted by comparing the ranked gene signature of NRG1 in NRG1-treated Lgr5^{med}-CD24^{low} cells *vs* untreated Lgr5^{med}-CD24^{low} cells with the stem cell signature published by Munoz *et al.* (Munoz et al., 2012). This analysis revealed a major shift in progenitor cell identity towards a stem cell-like state (Figure 6D). This could be the result of a delay in differentiation. This was validated in tissues where we observed strong *Olfm4* and

CD44v6 staining at the crypt bottom following NRG1 treatment in mice (Figure 6E and 6F). FACS analysis using two stem cell markers CD44 and EPHB2 (Jarde et al., 2015) revealed a population shift in NRG1-treated stem cells (Figure 6G). In NRG1-treated mice, a more homogeneous cell population was evident with 97% of Lgr5^{high}-CD24^{low} cells expressing high levels of CD44 and EPHB2 compared to 75% of stem cells in controls (Figure 6G).

We then investigated if these changes in cell identity translated to functional changes. Stem cells (Lgr5-GFP^{high}) and progenitor daughter cells (Lgr5-GFP^{med} and Lgr5-GFP^{low}) were isolated at the single cell level from Lgr5-EGFP mice by FACS and subjected to an organoid formation assay which evaluates the ability of single cells to form new organoids in order to assess their stem cell potential (Mihaylova et al., 2018; Serra et al., 2019). In ENR medium, Lgr5-GFP^{high} cells generated more organoids than Lgr5-GFP^{med} and Lgr5-GFP^{low} cells as expected (Figure 6H). NRG1 treatment dramatically increased (by 50%) the ability of Lgr5-GFP^{high}, Lgr5-GFP^{med} and Lgr5-GFP^{low} cells to form organoids compared to EGF (Figure 6H). Interestingly, the organoid forming efficiency of NRG1-stimulated Lgr5-GFP^{med} cells was not significantly different to Lgr5-GFP^{high} stem cells cultured with EGF (Figure 6H). Similar phenotypes were observed when single cells were supplemented with NRG1 in the absence of EGF (Figure S7E).

These results clearly demonstrate that NRG1 promotes a proliferative signature in stem and progenitor cells and induces these cells to express higher levels of stem cell markers. Furthermore, this correlates to augmentation of functional activity as demonstrated by the increased capacity of NRG1-treated progenitor cells to initiate organoid cultures and support subsequent growth.

NRG1 treatment boosts proliferation and regeneration of the intestinal epithelium following damage

To investigate whether NRG1 treatment could improve stem cell-mediated regeneration, mice were challenged with the chemotherapeutic drug 5-FU to induce crypt damage and then treated with NRG1 (Figure 7A). NRG1-treated animals had longer villi (+16%) and the number of crypts and proliferative BrdU+ cells per field of view was significantly increased (Figure 7B and 7C). This was recapitulated *in vitro* where organoids treated with NRG1 exhibited a dramatic increase in complexity with multiple buds, which are similar to *in vivo* crypt domains (Figure 7D and 7E). The percentage of low budding organoids (0-2 crypt units) was decreased by 40% and, conversely, the percentage of advanced organoids (≤7 crypt domains) was

increased by 42% in cultures supplemented with NRG1 (Figure 7D and 7E). Finally, the ability of NRG1 treatment to promote stem cell reoccurrence following injury was examined. Expression of the stem cell markers *Hes-1, Lgr5, Olfm4* and *Smoc2* was up-regulated in NRG1-treated tissues (Figure 7F). To rule out the fact that up-regulation of these markers was only due to an increase in the total number of crypts, we analysed expression of *Olfm4* in regenerating tissue treated with NRG1. An intense *Olfm4* signal was detected by *in situ* hybridisation at the base of intestinal crypts where an expansion of the *Olfm4*+ stem cell compartment was evident (Figure 7G). The number of OLFM4+ cells per field of view was robustly increased by 45% in NRG1-treated mice compared to controls (Figure 7H).

These observations show that despite the endogenous elevation of NRG1 during regeneration, further treatment with NRG1 enhanced intestinal tissue regeneration by increasing crypt density, cell proliferation and the efficient reappearance of the stem cell pool.

Discussion

Previous studies have highlighted the importance of WNT and EGF signalling in maintaining ISCs during normal homeostasis and the rapid proliferative response required to repair damage following injury (Farin et al., 2012; Horvay et al., 2011; Horvay et al., 2015; Kabiri et al., 2014; Koch, 2017; Lee et al., 2008; Mah et al., 2016; Pejchal et al., 2015). Multiple reports have now demonstrated that *in vivo* WNTs, R-spondins and regulators of BMP signalling are secreted from stromal cells underlying the crypt compartment (Degirmenci et al., 2018a; Greicius et al., 2018; McCarthy et al., 2020; Stzepourginski et al., 2017; Valenta et al., 2016). However, the nature and cell source of secreted signals that drive regeneration following injury is less clear. Here, we have identified NRG1 as a mesenchymal niche-derived signal that supports the proliferation of stem and progenitor cells in the regenerating epithelium by activation of MAPK and PI3K-AKT signalling.

Fundamental studies in the *Drosophila* intestinal tract using bacterial infection to induce damage has revealed the EGF signalling pathway is required for cell proliferation in the regenerative tissue response (Buchon et al., 2010). The EGF ligand *vein (vn)* is dramatically up-regulated in muscle underlying the intestinal epithelium following damage (Jiang et al., 2011) and provides a permissive signal to ISCs which then allows cell proliferation to be driven by JAK/STAT signalling (Biteau and Jasper, 2011). These studies support a model where the visceral muscle is a functional niche in *Drosophila* which secretes *vn* following tissue damage or stress to stimulate a tissue repair response.

Although Paneth cells secrete niche ligands that can interact with ISCs in the mammalian gut, it is evident that *in vivo*, signals from the epithelium are dispensable for homeostasis and regeneration (Farin et al., 2012; Kabiri et al., 2018; Valenta et al., 2016). In contrast, the stromal compartment of the intestinal tract has been shown to supply key WNT and BMP signalling agonists and antagonists to generate a gradient of signalling activity along the crypt villus axis. A variety of mesenchymal cell sources have been described including FOXL1+ (Aoki et al., 2016; Shoshkes-Carmel et al., 2018), PDGFRα+ (Greicius et al., 2018; McCarthy et al., 2020), CD34+ (Stzepourginski et al., 2017), Gli1+ (Degirmenci et al., 2018b) and Grem1+ (McCarthy et al., 2020) cell populations. Genetic ablation of many of these cell types produce profound epithelial defects, providing evidence of their role as critical niche components. Numerous studies have also suggested SMA-positive myofibroblasts may constitute the niche and have demonstrated the ability of these cells to support organoid growth without the addition of WNT agonists (Kabiri et al., 2014; Lahar et al., 2011; Valenta et al., 2016). Single cell sequencing

has recently identified three distinct PDGFRα+ mesenchymal cell populations which has further clarified the contribution of different niche cells. PDGFRα^{high} FOXL1+ telocytes express numerous BMP and WNT regulators, while two PDGFRα^{low} CD34+ stromal populations also express WNT signalling molecules. Interestingly, one of the PDGFRα^{low} populations referred to as trophocytes, localise under crypts and can support growth of organoids ex vivo (McCarthy et al., 2020). NRG1 is clearly expressed in multiple mesenchymal populations, including macrophages and PDGFRα+ cells. This includes the SMA-negative sub-epithelial mesenchymal telocyte population described by Shoshkes-Carmel et al. (2018) and CD11b+ CSF1R-dependent gut macrophages that reside in close proximity to crypts (De Schepper et al., 2018) and when depleted, result in loss of *Lgr5*-positive ISCs (Sehgal et al., 2018). The relative numbers of these cells do not change dramatically following injury but the expression of NRG1 is strongly elevated. Most notably, CD34+ PDGFRα+ cells switch on NRG1 during regeneration suggesting activation of these cells in the repair process. Our data confirm that CD34+ cells express lower levels of PDGFRα and are located in stroma surrounding crypts, so likely correspond to the trophocyte/stromal cells identified by McCarthy et al. (2020). Our studies here clearly implicate NRG1 as a key niche signal that is switched on in stromal cells surrounding crypts to promote regeneration. This is reminiscent of up-regulation of *vn* during regeneration of the *Drosophila* gut suggesting this is an evolutionary conserved process.

Intriguingly, NRG1, not EGF, was up-regulated in mesenchymal tissue during regeneration following epithelial damage. This observation strongly implicates NRG1 as having a more specific role in modulating tissue response following injury. This was reinforced by assays in organoid culture where NRG1 could not only replace EGF in the culture medium, but could more potently enhance cell division and activation of AKT/MAPK signalling. Furthermore, NRG1 promoted further cell proliferation even when EGF was present. It is likely that there is some level of redundancy in the function of EGFR/ERBB receptor family and activating ligands in the intestinal epithelium as demonstrated by previous studies (Lee et al., 2009; Lee et al., 2008; Luetteke et al., 1999; Srivatsa et al., 2017; Threadgill et al., 1995). Here, we show that EGF and NRG1 likely both contribute to epithelial homeostasis, but identify NRG1 as a key endogenous agonist of the EGF family that acts during epithelial repair.

Lgr5+ cells are rapidly lost following insult with chemotherapy or radiation exposure (Metcalfe et al., 2014; Tian et al., 2011) and lineage tracing studies have shown considerable plasticity in progenitor cell populations where both secretory and absorptive precursors can de-differentiate to replace the lost Lgr5+ cells (Ayyaz et al., 2019; Buczacki et al., 2013; Murata et al., 2020;

Nusse et al., 2018; Tetteh et al., 2016; Tian et al., 2011; van Es et al., 2012; Wang et al., 2019; Yui et al., 2018). R-spondin 3 contributes to this process (Harnack et al., 2019), but other niche signals that drive this process have not been identified. Our results here show that exposure of FACS-sorted progenitor cells to NRG1 *in vitro* converts the identity of progenitor cells towards a more stem-like phenotype and endows an increased organoid-initiating capacity to progenitors that is equivalent to non-treated Lgr5+ stem cells. Analysis of receptor phosphorylation determined that ERBB3 and ERBB2 are activated by NRG1 in intestinal organoids to promote budding that is dependent on WNT signalling, but is less dependent on EGFR. Overall, this supports the concept that NRG1 drives progenitor cells with an activated WNT pathway back towards a functional stem cell state to enhance regeneration.

In summary, this study has identified NRG1 as a potent promoter of stem cell identity that acts endogenously to enhance the repair of intestinal epithelium following damage. Furthermore, NRG1 is more effective at supporting stem cell activity and proliferation in SI organoid cultures than EGF. This has potential applications for the development of strategies for the treatment of conditions such as necrotising enterocolitis, ulcerative colitis, Crohn's disease and short gut syndrome characterised by injury and epithelial deficiency.

Limitations of Study

Although our study demonstrates the role of NRG1 during tissue regeneration, and defines some differences in function compared to EGF, we did not evaluate the function of other members of the EGF family of ligands. It is possible that these ligands, in conjunction with NRG1, contribute to supporting intestinal tissue regeneration following injury. To further scrutinise the role of NRG1 during the early stages of tissue regeneration, it would be insightful to conduct *in vivo* lineage tracing from progenitor cells and examine the dynamics of de-differentiation of these cells into new intestinal stem cells. Furthermore, although we observed activation of both MAPK and AKT following NRG1 stimulation, it remains to be elucidated whether these two signalling pathways jointly or independently contribute to the impacts observed.

Acknowledgements: The authors acknowledge the resources and staff of the BDI Organoid Program, Micro Imaging, Flowcore, MARP and Histology platforms at Monash University, Victoria, Australia. We also thank the ACRF Centre for Cancer Genomic Medicine at the MHTP Medical Genomics Facility (Clayton, Australia) and Dr Chappaz for help with

flow cytometry. This work is supported by NHMRC Australia grants 1129600 (TJ), 1011187, 1100531 (HEA), 1188689 (HEA, TJ), Monash University grant (TJ, HEA), MRC, UK MR/R026424/1(TJP), BLS/CMU Fellowship (TJP), Sylvia and Charles Senior Medical Viertel Fellowship (JMP), Monash BDI scholarship (EC) and a RTP scholarship (TKK). We thank Prof Hans Clevers for helpful discussions.

Author Contributions: TJ and HEA designed this study. TJ, WHC and HEA wrote the manuscript. TJ, HEA, WHC, TKK, FJR, MT, CMN, TKA, DRP, GK, RME, TF, MG, ER, EC, MP and JFD have performed the experiments, analysed and compiled the data. JMP, SA, RJD, PJM and TJP have provided valuable expertise, data interpretation, reagents and analysis tools. All authors have read and edited the manuscript.

Declaration of Interests. The authors declare no competing interests.

Figure titles and legends

Figure 1. Niche-derived NRG1 is up-regulated during regeneration and promotes *in vitro* organoid proliferation

(A) qRT-PCR analysis of *Lgr5* and *Olfm4* (stem cell markers) compared with *Nrg1* and *Egf* expression in the SI at 0, 2, and 5 days following irradiation shows *Nrg1* is up-regulated during regeneration. (n=6 per time point, Kruskal-Wallis one-way ANOVA, *, $p<0.05$, *vs* day 0).

(B) Immunostaining for NRG1 (red) in SI at days 0 and 5 post-irradiation demonstrates elevation of NRG1 in the mesenchyme (n=3, DAPI, blue). Crypt domains are outlined. Scale bar, 50 µm.

(C) qRT-PCR analysis of *Lgr5*, *Olfm4*, *Nrg1* and *Egf* expression in SI at 0, 2, 5, and 7 days post 5-FU treatment (n=6 per time point, Kruskal-Wallis one-way ANOVA, *, $p<0.05$, *vs* day 0).

(D) Immunostaining for NRG1 (red) in the SI post-5-FU treatment shows upregulation during regeneration (n=3, DAPI, blue). Crypt domains are outlined. Scale bar, 50 µm.

(E) SI organoids cultured in EGF, NRG1 or both for 5 days demonstrates that NRG1 enhances organoid growth (n=6). Scale bar, 100 µm.

(F) Organoid sections stained with H&E and immunostained for BrdU (n=3) following culture in the presence of EGF, NRG1 or both for 5 days shows an increase in proliferation. Scale bar, 70 µm.

(G) Quantification of organoid growth in EGF, NRG1 or both after 4 days shows an increase in growth with NRG1 (n=6, One-way ANOVA, *, $p<0.05$). For all conditions, R-spondin 1 and Noggin were added.

(H) Western blot analysis shows an increase in pAKT, and pERK, in SI organoids supplemented with NRG1 compared to EGF after starvation of EGF for 5 hours (n=3, Paired Student T test, *, $p<0.05$). Images are composites of an individual image that have been cropped and stitched together.

For all graphs, bars represent mean ± SEM.

See also Figure S1.

Figure 2. NRG1 is localised in mesenchymal and epithelial niche cell populations and is up-regulated during regeneration

(A) qRT-PCR analysis of *Nrg1* expression in purified mesenchymal cell populations from control, 13 Gy irradiated and 5-FU treated mice at day 5 shows NRG1 is upregulated in mesenchymal cells following injury (n=6, Unpaired Student T test, *, $p<0.05$, *vs* control).

(B) Co-immunofluorescent staining for NRG1 (red) and F4/80 or PDGFRα (green) in SI tissues at days 0 and 5 post-irradiation demonstrates that sub-sets of these cells (white arrows) express NRG1 (n=3). Crypt domains are outlined. Scale bar, 50 µm.

(C) qRT-PCR analysis of *Egf* expression in cell populations from control, irradiated and 5-FU treated mice at day 5 (n=6, Unpaired Student T test, *, $p<0.05$, *vs* control).

(D) Immunofluorescent detection of NRG1 (red) or ERBB3 (red) and Lgr5-GFP (green) in SI tissues (n=3). NRG1-positive cells (white arrows) do not co-localise with Lgr5-GFP cells in crypts. ERBB3-positive cells (white arrows) co-localise with Lgr5-GFP cells. Crypt domains are outlined. Scale bar, 10 µm.

For all graphs, bars represent mean ± SEM.

See also Figures S2 and S3.

Figure 3: Loss of NRG1 impairs regeneration following injury

(A) Induction protocol for deletion of *Nrg1* in the SI. Control (Ubc-Cre-ER^{T2+} *Nrg1*$^{+/+}$) and *Nrg1* KO (Ubc-Cre-ER^{T2+} *Nrg1*$^{fl/fl}$) are compared. Tissue analyses are conducted at day 16.

(B) Knockout of *Nrg1* is verified by the reduction of *Nrg1* mRNA by qRT-PCR (n=7).

(C) BrdU immunostaining shows reduced levels in Nrg1 KO animals. Scale bar, 20 µm.

(D) Quantification of BrdU+ cells and BrdU+ CBC stem cells reveals a reduction of these cells following *Nrg1* KO (n=7-8).

(E) Cells expressing *Olfm4* are reduced following *Nrg1* KO as examined by *in situ* hybridisation (n=7-8). Scale bar, 20 µm.

(F) Induction protocol for deletion of *Nrg1* followed by irradiation-induced injury and collection of tissues at day 16 (day 5 post-injury). Ubc-Cre-ER^{T2} *Nrg1*$^{+/+}$ (control) and Ubc-Cre-ER^{T2} *Nrg1*$^{fl/fl}$ (Nrg1 KO) mice were compared for all analyses.

(G) Knockout of *Nrg1* using the protocol in 3F is verified by the reduction of *Nrg1* mRNA by qRT-PCR (n=3-4).

(H) BrdU staining of tissue from irradiated control and *Nrg1* KO animals reveals a decline in proliferative cells. Scale bar, 50 µm.

(I) Quantification of BrdU+ cells per field of view and per crypt in control and *Nrg1* KO mice reveals a significant decrease in the proliferation (n=3-4).

(J) OLFM4 immunostaining reveals a decrease in OLFM4+ cells per crypt during regeneration following irradiation in *Nrg1* KO mice (n=3-4). Scale bar, 50 µm.

(K) Induction protocol for deletion of *Nrg1* followed by 5-FU-induced injury. Tissues are analysed at day 16 (day 4 post-injury).

(L) Knockout of *Nrg1* is verified by the reduction of *Nrg1* mRNA by qRT-PCR (n=5).

(M) BrdU immunostaining of tissue following 5-FU-induced injury reveals reveal a reduction in the proliferation. Scale bar, 100 µm.

(N) Quantification of BrdU+ cells per field of view in control and *Nrg1* KO mice (n=5) shows a significant reduction of proliferating cells.

(O) OLFM4 immunostaining reveals a reduction in ISCs in regenerating crypts when *Nrg1* is depleted (n=5). Scale bar, 50 µm.

All statistical analyses utilised the unpaired Student T test, *, $p<0.05$, *vs* control. All bars represent mean ± SEM.

See also Figures S4 and S5.

Figure 4. NRG1 treatment promotes cell proliferation and regulates intestinal stem and progenitor cells

(A) NRG1 supplementation strategy over 5 days to examine the regenerative effect of NRG1 in the SI. Vehicle injected animals were used as controls and tissues were harvested at day 6.

(B) H&E-stained SI sections revealed the presence of elongated crypts in NRG1-treated mice (n=8).

(C) BrdU-stained SI tissue reveals NRG1-treatment promotes proliferation in crypts (n=8).

(D) qRT-PCR analysis of stem cell markers *EphB2*, *Hes-1*, *Lgr5*, *Olfm4* and *Smoc-2* show up-regulation following NRG1 treatment (n=4-5).

(E) NRG1 supplementation strategy using Lgr5-EGFP mice (n=3). Cells from four populations ($Lgr5^{-}$ $CD24^{-}$, Lgr5-GFP^{low} $CD24^{low}$, Lgr5-GFP^{med} $CD24^{low}$ and Lgr5-GFP^{high} $CD24^{low}$) were isolated by FACS on day 6 for molecular analyses.

(F) Heatmap of RNA sequencing data shows differences in gene expression in the four FACS-sorted populations (average of three datasets for each group) in NRG1 versus vehicle controls.

(G) Differentially expressed genes in NRG1-treated mice compared to controls.

(H) Brightfield and KI-67 stained SI organoids following treatment for 4 days with IWP2, DAPT or verteporfin in organoid medium supplemented with EGF or NRG1 (n=3). Scale bar, 100 µm.

(I) Quantification of cells in organoids treated with inhibitors (n=3, one-way ANOVA, *, $p<0.05$).

Scale bars for all histological sections, 20 µm. Graphs in B, C, D all utilise the unpaired Student T test (*, $p<0.05$, *vs* control). All bars represent mean ± SEM.

See also Figures S6.

Figure 5: NRG1 drives a proliferative signature in stem and progenitor cells

(A) Gene ontology analysis of the differentially expressed genes for the four FACS- sorted cell populations from NRG1-treated Lgr5-EGFP mice show an increase in cell cycle and mitotic processes in Lgr5-GFP^{high} and Lgr5-GFP^{med} cells.

(B) Fluorescent images of SI sections from Lgr5-GFP mice co-stained for BrdU reveals NRG1-treatment increases proliferation of stem cells. Scale bar, 20 µm. n=3, Unpaired Student T test, *, $p<0.05$, *vs* control. Bars represent mean ± SEM.

(C) Violin plots for cell proliferation markers assessed by single cell PCR in 30 double-sorted Lgr5-GFP^{high} cells (Kolmogorov–Smirnov test, *, $p<0.05$, *vs* control) reveal more homogenous populations are present following NRG1 treatment.

Figure 6. NRG1 supports stem cell identity and partial progenitor cell reversion

(A-C) Lgr5-GFP mice treated with NRG1 (n=3) and FACS sorted into stem and progenitor populations (see Figure 4E and S3D).

(A) Principal component analysis of the RNA sequencing data shows control (blue) and NRG1-treated (red) animals. Average of three datasets are shown for each group.

(B) Unsupervised hierarchical clustering analysis of genes differentially expressed in NRG1-treated and control Lgr5-GFP^{med} cells.

(C) Analysis of ISC markers in Lgr5-GFP^{med} and Lgr5-GFP^{high} cells reveals NRG1-treatment promotes expression of ISC markers. Bars represent fold change calculated based on the ratio of change when comparing two conditions composed of three biological replicates (FDR<0.05, genes expressed at >2 fold higher levels in both NRG1-treated Lgr5^{med}-CD24^{low} and untreated Lgr5^{high}-CD24^{low} cells compared to untreated Lgr5^{med}-CD24^{low} cells, p-value of the significance of the fold change < 10^{-4}).

(D) Gene Set Enrichment Analysis of the gene signature in NRG1-treated Lgr5^{med} *vs* control Lgr5^{med}-CD24^{low} cells shows enrichment of ISC genes (stem cell signature by Munoz et al., 2012).

(E) *Olfm4 in situ* reveals elevation of expression following NRG1 treatment (n=4). Scale bar, 20 µm.

(F) Immunostaining for CD44v6 reveals enhanced staining at the base of SI crypts following NRG1 treatment (n=4). Scale bar, 10 µm.

(G) Flow cytometry shows more homogeneous populations of cells highly expressing the stem cell markers CD44 and EPHB2 following NRG1-treatment (n=4, Unpaired Student T test, *, p<0.05).

(H) Isolated single Lgr5-GFP stem and progenitor cells generate more organoids and overall cell numbers when cultured in the presence of NRG1 for 5 days. Scale bar, 500 µm. Bars represent mean ± SEM (n=3, Paired Student T test, *, p<0.05).

See also Figure S7.

Figure 7. NRG1 augments regeneration following damage and supports establishment of ISCs

(A) Strategy for examining if NRG1 can enhance the regenerative response following injury induced by 5-FU.

(B) H&E-stained SI tissue from 5-FU injured mice reveals NRG1-treatment induces a significant increase in crypt and villus length (n=8). Scale bar, 100 µm.

(C) BrdU-stained SI from 5-FU injured mice shows NRG1-treatment increases the number of proliferative cells (n=7-8). Scale bar, 20 µm.

(D) Images of intestinal organoids cultured in the presence of EGF or NRG1 or both for 6 days (n=3) demonstrate that NRG1 promotes budding. Scale bar, 200 µm.

(E) Quantification of crypt domains in intestinal organoids treated with EGF and NRG1 or both for 6 days (n=3, Paired Student T test, *, $p<0.05$).

(F) qRT-PCR analysis of *EphB2*, *Hes-1*, *Lgr5*, *Olfm4* and *Smoc-2* shows NRG1 treatment causes up-regulation of stem cell markers (n=7-8).

(G) *Olfm4* in situ hybridisation shows an increase in expression following 5-FU challenge and NRG1 treatment (n=5). Scale bar, 20 µm.

(H) Immunostaining for OLFM4 shows an increase in the number of OLFM4+ cells following 5-FU challenge and NRG1 treatment (n=6-8). Scale bar, 50 µm.

Graphs shown utilise the unpaired Student T test (* $p<0.05$, *vs* control), unless indicated. Bars represent mean ± SEM.

STAR Methods

RESOURCE AVAILABILITY

Lead Contact

Further information and requests for resources and reagents should be directed to and will be fulfilled by the Lead Contact, Helen E. Abud (helen.abud@monash.edu).

Materials Availability

This study did not generate new unique reagents.

Data and Code Availability

The datasets generated during this study are available at GEO (GSE149311).

EXPERIMENTAL MODEL AND SUBJECT DETAILS

Transgenic animal models

Male and female adult Lgr5-eGFP-IRES-CreERT2 (Barker et al., 2007), Villin-Cre-ERT2 (el Marjou et al., 2004) Ubc-CRE-ERT2 (Ruzankina et al., 2007) *Nrg1*$^{fl/fl}$ (Zhang et al., 2011) ROSA26-ZsGreen1 (Madisen et al., 2010) and wild-type C57BL/6 mice were used for experiments (8–14 week old). Animals were housed at the animal facility (Monash Animal Services, Clayton, Australia) in strict accordance with good animal practice as defined by the National Health and Medical Research Council (Australia) Code of Practice for the Care and Use of Animals for Experimental Purposes. Experimental procedures were approved by the Monash Animal Research Platform (MARP) Animal Ethics Committee. Animals were maintained under a 12/12 light/dark cycle at a temperature of 20ºC with free access to food and water. The studies were designed using both male and female mice using group sizes determined by requirements to obtain statistically significant results as assessed by the MARP ethics committee.

To study epithelial repair of the intestine, wild-type C57BL/6 mice were challenged with a 13 Gy whole body irradiation or exposed to 5-fluorouracil (single intra-peritoneal injection, Sigma-Aldrich, #F6627, 150mg/kg body weight).

To induce loss of Nrg1 in the intestinal epithelium, Villin-Cre-ERT2 *Nrg1*$^{fl/fl}$ and Villin-Cre-ERT2 *Nrg1*$^{+/+}$ C57BL/6 mice were injected with one intra-peritoneal dose of tamoxifen (Sigma-Aldrich, #T5648, 80mg/kg) daily for 4 days. Tissues were then collected on day 5, 2 hours after a BrdU pulse (single intra-peritoneal injection, Sigma-Aldrich, #B5002, 80mg/kg).

To induce Nrg1 knock-out in both mesenchymal and epithelial intestinal cell compartments, Villin-Cre-ERT2 Ubc-Cre-ERT2 *Nrg1*$^{fl/fl}$ and Villin-Cre-ERT2 Ubc-Cre-ERT2 *Nrg1*$^{+/+}$ mice were injected with one intra-peritoneal dose of tamoxifen (Sigma-Aldrich, #T5648, 80mg/kg) daily for 5 days. Tissues were then collected on day 16, 2 hours after a BrdU pulse (single intra-peritoneal injection, Sigma-Aldrich, #B5002, 80mg/kg).

To induce Nrg1 signalling activation in the intestine, wild-type C57BL/6 and Lgr5-eGFP-IRES-CreERT2 C57BL/6 mice were injected with two intra-peritoneal doses of Nrg1 (R&D, #5898-NR) or vehicle control (PBS) daily (every 12 hours) for 5 days (male littermates were randomly assigned to experimental groups). Tissues were then collected on day 6, 2 hours after a BrdU pulse (single intra-peritoneal injection, Sigma-Aldrich, #B5002, 80mg/kg).

Organoid culture

As previously described (Horvay et al., 2015; Jarde et al., 2018) the murine small intestinal tube was dissected out and flushed with PBS to remove faeces. Small intestinal tissues were opened longitudinally, scraped with a glass coverslip to remove villi, cut into 5-mm pieces and washed with PBS five times to remove unattached epithelial fragments, mucus and faeces. Following incubation for 30 min at 4°C in 4mM EDTA-PBS solution, intestinal crypts were released from small intestinal tissue fragments by mechanically pipetting them with a 10 mL pipette in PBS and repeating this step three times. Intestinal crypts were strained (70 μm cell strainer, BD Biosciences) and centrifugated three times at 1500 rpm for 2 min at 4°C. Freshly isolated crypts were then mixed with 20μl of growth factor-reduced Matrigel (Corning), seeded in 48-well plates, and 500μl of crypt culture medium was overlaid [DMEM/F12 (Gibco) supplemented with N2 (Gibco), B27 (Gibco), penicillin/streptomycin (Gibco), glutamax (Gibco), 10 mM HEPES (Gibco), fungizone (Gibco), 50 ng/mL EGF (Peprotech, #315-09), 100 ng/mL Noggin (Peprotech, #250-38) and 500 ng/mL R-spondin 1 (Peprotech, #120-38) or 10% R-spondin 1 conditioned media]. Human recombinant NRG1 (R&D, #5898-NR) was supplemented at a concentration of 100 ng/mL. Intestinal organoids were maintained in a 37°C humidified atmosphere under 5% CO2 and medium was replaced every 2 days.

For *Nrg1* deletion experiments, organoids generated from Villin-Cre-ERT2 *Nrg1*$^{fl/fl}$ and Villin-Cre-ERT2 Nrg1$^{+/+}$ small intestinal tissues were established. After 7 days in culture, organoids were mechanically passaged and 150 crypt fragments were seeded per 48-well plate well. Nrg1 gene deletion was induced by treating Villin-Cre-ERT2 *Nrg1*$^{fl/fl}$ and Villin-Cre-ERT2 Nrg1$^{+/+}$

organoids with 100 nM 4OH-tamoxifen (Sigma Aldrich, #T176) in the culture medium for 4 days.

For inhibitor experiments, wild-type small intestinal organoids were mechanically passaged and 150 organoid fragments per well replated in Matrigel in a 48 well plate. Organoid fragments were then exposed to complete medium containing 10% R-spondin 1 conditioned media, 100 ng/mL Noggin, 100 ng/mL EGF or 100 ng/mL NRG1 supplemented with 10 µM DAPT (Sigma-Aldrich, #D5942), 250 nM gefitinib (Sigma-Aldrich, #SML1657), 5 µM IWP2 (Sigma-Aldrich, #I0536) or 1 µM verteporfin (Sigma-Aldrich, #SML0534). After 2 days, the medium was replaced with fresh complete culture medium containing fresh inhibitors. The assessment of cell growth was then assessed at day 4. Organoids were exposed to Presto-Blue cell viability reagent (Thermo Fisher Scientific, #A13262) in the culture medium for 20 min at 37°C according to the manufacturer's instructions. Organoids were then processed for KI-67 immunofluorescence staining.

Single cell organoid culture

Following FACS isolation (described in 'FACS isolation of intestinal epithelial cells'), single epithelial cells were collected in DMEM/F12 supplemented with 10% serum and 10 µM Y-27632 (Abcam). As previously described (Jarde et al., 2018) intestinal cells were centrifugated at 4°C for 5 min at 1500 rpm. The cell pellet was resuspended in growth-factor reduced Matrigel (1000 cells per µl, Corning). 5000 cells were seeded per well in a 96 well plate. Following Matrigel polymerization, 100 µl of crypt culture medium per well was overlaid [DMEM/F12 (Gibco) supplemented with N2 (Gibco), B27 (Gibco), penicillin/streptomycin (Gibco), glutamax (Gibco), 10 mM HEPES (Gibco), fungizone (Gibco), 50 ng/mL EGF (Peprotech, #315-09), 100 ng/mL Noggin (Peprotech, #250-38), 1 µg/mL R-spondin 1 (R&D Systems, #120-38), 10 µM Y-27632 (MedChemExpress, #HY-10583), 1 µM jagged-1 (Anaspec, #AS-61298), 100 ng/mL WNT-3a (Peprotech, #315-20), 2.5 µM CHIR (Stemgent, #04-0004) +/- 100 ng/mL NRG1 (R&D Systems, #5898-NR)]. Intestinal cells were maintained in a 37°C humidified atmosphere under 5% CO2. After 3 days, the culture medium was entirely replaced by freshly made culture medium without Y-27632 and Wnt-3a. After 4 days in culture, images of wells (5 wells per condition, 3-5 biological replicates) were taken, cell viability measured using the PrestoBlue Cell Viability kit (Thermo Fisher Scientific, #A13262) and organoids were manually counted using FIJI image analysis cell counter software (Schindelin et al., 2012).

Mesenchymal fibroblast culture

After performing crypt isolation, epithelium deprived small intestinal tissues were incubated with 0.31 mg/mL dispase type 2 (Sigma Aldrich, # D4693) and 0.375 mg/mL collagenase A (Roche, # 10103586001) in DMEM/F12 at 37°C for 1 hour. Mesenchymal cells were released from small intestine tissue fragments by mechanically pipetting them with a 10 mL pipette. The solution was strained with a 70µm cell strainer (BD Biosciences) and centrifugated at 4°C at 1500 rpm for 3 min. Mesenchymal cells were then resuspended in DMEM containing 10% serum (Gibco), glutamax (Gibco) and penicillin/streptomycin (Gibco), transferred in a T25 flask (Falcon) and maintained in a 37°C humidified atmosphere under 5% CO2. The culture medium was replaced every 2 days.

Human small intestinal tissue

Normal human small intestinal tissues from adult patients were collected following surgery at Cabrini Hospital (Malvern, Victoria). The study was approved by the Cabrini Human Research Ethics Committee (reference #05-11-04-11). All patients provided written informed consent.

METHOD DETAILS

Immunohistochemistry and co-immunofluorescence

As previously described (Horvay et al., 2011; Mileto et al., 2020), tissues from the medial part of the mouse small intestine were swiss-rolled, fixed in 4% paraformaldehyde, paraffin embedded and cut into 4 µm sections. Normal human small intestinal tissues were fixed in 4% paraformaldehyde, paraffin embedded and cut into 4 µm sections. Slides were deparaffinised in xylene, rehydrated in graded alcohols and incubated in citrate buffer solution (pH=6) for 10 min in a pressure cooker. Slides were then blocked with 1% hydrogen peroxide for 5 min and CAS block (Life Technologies - #008120) for 1 hour at room temperature before incubation overnight at 4°C with primary antibodies (anti-BrdU - BD Biosciences - #555627; anti-CD44v6 - eBioscience - #BMS145; anti-ERBB3 - Cell Signaling - #12708; anti-KI-67 - Abcam - #ab15580; anti-Lysozyme - DAKO - #A0099; anti-NRG1 - Santa Cruz - #sc-348; anti-OLFM4 - Cell Signaling - #39141; anti-Synaptophysin - DAKO - #M0776). Slides were washed and then exposed to anti-mouse or anti-rabbit horseradish peroxidase conjugated antibodies (Life Technologies, 1:200) in PBS with 1% bovine serum albumin for 1 hour at room temperature. Peroxidase activity was detected with the 3, 3'-diaminobenzidine liquid kit (Dako - #K3468). Sections were counterstained with haematoxylin, dehydrated and mounted.

Morphometric analysis and cell counts were performed using the Aperio ImageScope software and FIJI image analysis cell counter software counting at least 25 crypt/villus units per tissue section (Schindelin et al., 2012).

For immunofluorescence, slides were treated as described above and were incubated overnight with primary antibodies (anti-BrdU - BD Biosciences - #555627; anti-ERBB3 - Cell Signalling - #12708; anti-F4/80 – Bio-Rad - #MCA497GA; anti-GFP - Rockland - #600-101-215; anti-KI-67 – Abcam - #ab15580; anti-Lysozyme - Santa Cruz - #sc-27956; anti-NRG1 - Abcam - #ab191139; anti-NRG1 - Santa Cruz - #sc-348; anti-PDGFRα - R&D - #AF1062; anti-α smooth muscle actin - Sigma Aldrich #A2547). Slides were washed and then exposed to Alexa Fluor 488 donkey anti-goat IgG, Alexa Fluor 568 donkey anti-mouse IgG or Alexa Fluor 637 donkey anti-rabbit IgG (Invitrogen, 1/500) for 1 hour and counterstained with DAPI. Fluorescent images were taken on a Nikon C1 confocal microscope (Nikon, Japan). Illumination intensity, exposure, offset and gain settings were maintained between samples. For whole mount immunofluorescence on organoids, organoids in Matrigel were fixed in 4% paraformaldehyde for 30 minutes and washed 3 times in PBS followed by 3 washes with 100mM glycine in PBS. Organoids were subjected to 10% horse serum in IF buffer (0.1% bovine serum albumin, 0.2% Triton X-100, 0.05% Tween 20 in PBS) for overnight blocking. Organoids were then exposed to anti-KI-67 – Abcam - #ab15580 primary antibodies with 1% bovine serum albumin in PBS overnight at 4°C. Organoids were washed 2 times with IF buffer for 4 hours and then incubate overnight in IF buffer. Organoids were exposed to Alexa Fluor 488 donkey anti-rabbit IgG or Alexa Fluor 594 goat anti-rabbit IgG (Invitrogen, 1/500) for overnight and then counterstained with DAPI. Z-stack fluorescent and brightfield images were taken on a Leica DMi8 microscope (Leica, Germany). Illumination intensity, exposure, offset and gain settings were maintained between samples. Image analysis and Z-projection were performed using FIJI software and brightness and contrast settings were maintained between control and test images.

In Situ Hybridisation

Paraffin sections (8 µm) were dewaxed and hydrated in DEPC treated water/PBS and fixed in 4% PFA (10 min). Sections were subjected to Proteinase K treatment (30 µg/mL) for 15 min, post-fixed in 4% PFA for 10 min and washed 3 times in PBS. Acetylation of samples was performed by incubation in 0.1 M triethanolamine (pH=8.0) with 0.5% Acetic Anhydride for 15 min followed by three washes with PBS. Sections were air dried and pre-hybridised in

hybridisation solution (10 mM Tris pH=7.5, 600 mM NaCl, 1 mM EDTA, 0.25% SDS, 10% Dextran Sulfate, 1x Denhardt's, 200 µg/mL yeast tRNA, 50% Formamide) for 30 min at 65°C. Olfm4 probes were diluted in hybridisation buffer (150 ng per section) and incubated at 65°C for 24 hours. After removal of hybridisation solution, sections were washed once in 5x SSC, pH=7.5 at room temperature, once in 2x SSC for 20 min at 60°C, twice in 0.2x SSC for 20 min at 60°C and five times for 1 min in 1xMAB solution (100 mM Maleic Acid, 150 mM NaCl, pH=7.5) at room temperature before incubation in blocking solution (1x MAB with 20% serum and 1x BMB (Roche) for 1 hour. Anti-Digoxigenin antibody (Roche) (1/2000 dilution in blocking buffer) was prepared and sections were incubated overnight at 4°C. Finally, sections were washed five times in 1x MAB buffer for 5 min, twice in NTMT buffer (100 mM NaCl, 100 mM Tris pH=9.5, 50 mM MgCl2, 0.1 % Tween-20) and stained with NBT/BCIP solution (Life Sciences) at 4°C for up to 48 hours.

Western blotting

Proteins were isolated by resuspending intestinal organoids into RIPA lysis buffer. Equal amounts of cellular protein (80 µg) were separated on a 4-12% Bis Tris Gel (Invitrogen) and transferred onto nitrocellulose membranes. Immunoblotting in Figure S1G utilized antibodies against p-AKT (Santa Cruz, #sc-101629), AKT (Santa Cruz, #sc-1618), p-ERK (Santa Cruz, #sc-101761), ERK (Santa Cruz, #sc-94) and β-ACTIN (Thermo Fisher Scientific, #MS-1295) as a protein loading control. Immunoblotting in Figure 1H and S1H utilized antibodies against p-AKT (Cell Signaling, #4058), AKT (Cell Signaling, #4685), p-ERBB2 (Cell Signaling, #2247), ERBB2 (Cell Signaling, #2165), p-ERBB3 (Cell Signaling, #14525), ERBB3 (Cell Signaling, #4754), p-ERK1/2 (Cell Signaling, #4370), ERK1/2 (Cell Signaling, #4695) and TUBULIN (Sigma-Aldrich, #T5168) as a protein loading control. Quantification of band intensities was performed using Image Lab Software (Bio-Rad). Western blot images presented in Figure 1H and S1H are composites of an individual image that have been cropped and stitched together. Indeed, a third condition (no EGF no NRG1) was evaluated, but excluded from the final analysis.

Quantitative RT-PCR

Medial small intestinal tissues were homogenised and total RNA extracted using the Qiagen RNeasy mini kit (#74104). For intestinal organoids and sorted cells, total RNA was extracted using the Qiagen RNeasy micro kit (#74004). RNA was reverse transcribed using the QuantiTect Reverse Transcription kit (Qiagen - #205311). Quantitative reverse transcriptase

polymerase chain reaction (qRT-PCR) was performed using the QuantiNova SYBR Green PCR kit (Qiagen - # 208054). Triplicate samples were analysed on a LightCycler 480 machine (Roche Diagnostics). Gene expression levels were calculated using the 2-ΔCt method using the geometric mean of 2 housekeeping genes, β-actin and β-2-microglobulin. Primers are listed in Table S1.

FACS isolation of intestinal epithelial cells

Isolation of small intestinal crypts was performed as described in 'Organoid culture'. The collected crypts were maintained for 30 min at 4°C in DMEM/F12 – 10% serum (Gibco) and were then dissociated in TrypLE Express (Invitrogen) supplemented with 10 µM Rock inhibitor (Y-27632, Abcam) and DNAse 1 (Sigma-Aldrich) for 5 min at 37°C. Cell clumps and mucus were removed using a 70 µm cell strainer (BD Biosciences) and the remaining dissociated cells were washed twice with PBS collected by centrifugation at 4°C at 1500 rpm for 3 min.

Antibody labelling step as well as the final resuspension of the sample were performed with PBS supplemented with 2mM EDTA, 2% FBS and 10 µM Rock inhibitor (Y-27632). Cellularized crypts were incubated with anti-CD31-BV510 (1:200, clone: MEC 13.3, BD biosciences, #563089), anti-CD45-BV510 (1:200, clone: 30-F11, BD biosciences, #563891) and anti-CD24-PeCy7 (1:100, clone: M1/69, eBioscience, #25-0242-82) antibodies in a 500µl volume for 15 min on ice. After washing twice with PBS, the cells from one animal were resuspended in a final volume of 1 mL, passed through a 70 µm strainer and transferred into appropriate FACS tubes and propidium iodide (PI) added to a concentration of 2 µg/mL. Cell sorting was carried out with a 100 µm nozzle on an Influx instrument (BD Biosciences). Aggregates, debris, dead cells (PI+) and CD45+/CD31+ hematopoietic/endothelial contaminates were depleted. For the Lgr5-GFPhigh cell population, around 2% of the CD24low Lgr5-GFP brightest cells were selected. The subsequent 2% of the CD24low Lgr5-GFP+ cells were considered as Lgr5-GFPmed and Lgr5-GFPlow cell populations. Purity of collected fractions was confirmed by reanalysis of a small fraction of the sorted cells. For single cell applications, cells were double sorted.

FACS isolation of intestinal mesenchymal cells

Intestinal tissue fragments depleted of epithelial cells (as described in 'Organoid culture') were resuspended in digestion buffer containing 0.31 mg/mL Dispase II (Sigma-Aldrich, #D4693) and 0.375 mg/mL Collagenase (Sigma-Aldrich, #C5138) in DMEM-F12 for 1 hour at 37°C.

Intestinal tissues were then mechanically pipetted with a 10 mL pipette in PBS, strained (70 µm cell strainer, BD Biosciences) and centrifugated at 1500 rpm for 5 min at 4°C. Antibody labelling step as well as the final resuspension of the sample were performed with PBS supplemented with 2% FBS. Mesenchymal cells were incubated with anti-CD45-BV510 (1:200, BD biosciences, #563891), anti-EPCAM-FITC (1:200, BioLegend, #118208), anti-F4/80-PB (1:100, BioLegend, #123124), anti-CD11b-PE (1:500, BioLegend, #101208), anti-CD31-PeCy7 (1:200, eBiosciences, #25-0311-82), anti-GP38-ApcCy7 (1:200, BioLegend, #127418), anti-PDGFRα-APC (1:100, Biolegend, #135908) and anti-CD34-biotinlyated (1:150, eBiosciences, #13-0341-85) antibodies in a 250µl volume for 15 min on ice. Cells were washed with PBS and centrifugated at 1500 rpm for 5 min at 4°C. Mesenchymal cells were then incubated with a Streptavidin-conjugated BUV395 antibody (1:150, BD Biosciences, #564176) in a 250µl volume for 10 min on ice. After washing twice with PBS, the cells were resuspended in a final volume of 1 mL, passed through a 35 µm strainer and transferred into appropriate FACS tubes and propidium iodide (PI) added to a concentration of 2 µg/mL. Cell sorting was carried out with a 100 µm nozzle on an Influx instrument (BD Biosciences). The sorting strategy is described in detail in Figure S2.

Single cell PCR

Single cell PCR was performed as previously described (Nefzger et al., 2016) with LifeTechnologies Single Cell to Ct kit. 96-well plates for qPCR were filled with 10 µl lysis solution and single cells were deposited with a cell sorter into each well. As per kits instructions, cDNA was produced from the lysate and submitted to 18 cycles of preamplification with TaqMan probes (Life Technologies) of the five genes of interest (Aspm, Ccnb1, Foxm1, Ki67 and β-actin). Pre-amplified templates that were positive for the housekeeper β-actin (manually tested with qPCR) were then used for Single cell PCR data collection with a Biomark instrument (Fluidgm). Results are expressed as Log2Ex = LOD (Limit of Detection) Cq – Cq [Gene]. The limit of detection was set to 30. If Log2Ex value is negative, Log2Ex = 0. Thirty $CD24^{low}$ $Lgr5^{high}$ cells per group were used for analysis.

QUANTIFICATION AND STATISTICAL ANALYSIS

RNA-sequencing analysis

Libraries of each biological replicate were prepared with 15ng of RNA using the Nugen Ovation RNA-Seq system V2 kit followed by Nugen Ovation Ultralow System V2 kit. High

throughput sequencing was performed with HiSeq3000 with ~30 M reads targeted reads (single end 76nt length) per sample. In summary, sequencing adaptors and low quality reads were discarded using Trimmomatic [v 0.35] (Bolger et al., 2014) (Phred score of 6 consecutive bases below 15, minimum read length of 36nt). Sample sequencing reads were aligned to the complete mouse genome (GENCODE GRCm38 primary assembly) with STAR (version 2.4.2a) (Dobin et al., 2013) and transcripts quantified with featureCounts (exonic regions of GENCODE's vM4 annotation version) (Liao et al., 2014). Gene transcripts with more than 5 sequencing reads and 1 count per million of mapped reads in at least one library-sized normalized sample (TMM method) (Robinson and Oshlack, 2010) were used for further analysis. Differential gene expression and gene ontology (Biological process) analyses was performed using limma/voom (Phipson et al., 2016; Ritchie et al., 2015) or Limma/voom with sample weights (Liu et al., 2015) and Metascape respectively (Tripathi et al., 2015). Limma's plotMDS function was used to perform multidimensional scaling analysis and unsupervised hierarchical clustering were performed with hclust (Euclidean's distances calculated with bioDist's euc function, B. Ding, R. Gentleman and V. Carey (2017). bioDist: Different distance measures. R package version 1.50.0). Plots were generated using limma's plotMDS function, ggplots2 (H. Wickham. ggplot2: Elegant Graphics for Data Analysis. Springer-Verlag New York, 2009) and ComplexHeatmap (Zuguang Gu (2015). ComplexHeatmap: Making Complex Heatmaps. R package version 1.6.0, https://github.com/jokergoo/ComplexHeatmap) R packages.

Statistical analysis

Statistical significance ($p<0.05$) was determined using the Kruskal-Wallis one-way ANOVA, one-way ANOVA, Kolmogorov–Smirnov test or Unpaired/Paired Student T test in GraphPad Prism (version 7.03) depending on experimental design and according to the figure legends.

References

Abud, H.E., Watson, N., and Heath, J.K. (2005). Growth of intestinal epithelium in organ culture is dependent on EGF signalling. Experimental cell research *303*, 252-262.

Amit, I., Citri, A., Shay, T., Lu, Y., Katz, M., Zhang, F., Tarcic, G., Siwak, D., Lahad, J., Jacob-Hirsch, J.*, et al.* (2007). A module of negative feedback regulators defines growth factor signaling. Nat Genet *39*, 503-512.

Aoki, R., Shoshkes-Carmel, M., Gao, N., Shin, S., May, C.L., Golson, M.L., Zahm, A.M., Ray, M., Wiser, C.L., Wright, C.V.*, et al.* (2016). Foxl1-expressing mesenchymal cells constitute the intestinal stem cell niche. Cellular and molecular gastroenterology and hepatology *2*, 175-188.

Ayyaz, A., Kumar, S., Sangiorgi, B., Ghoshal, B., Gosio, J., Ouladan, S., Fink, M., Barutcu, S., Trcka, D., Shen, J.*, et al.* (2019). Single-cell transcriptomes of the regenerating intestine reveal a revival stem cell. Nature *569*, 121-125.
Barker, N., van Es, J.H., Kuipers, J., Kujala, P., van den Born, M., Cozijnsen, M., Haegebarth, A., Korving, J., Begthel, H., Peters, P.J.*, et al.* (2007). Identification of stem cells in small intestine and colon by marker gene Lgr5. Nature *449*, 1003-1007.
Bartus, K., Galino, J., James, N.D., Hernandez-Miranda, L.R., Dawes, J.M., Fricker, F.R., Garratt, A.N., McMahon, S.B., Ramer, M.S., Birchmeier, C.*, et al.* (2016). Neuregulin-1 controls an endogenous repair mechanism after spinal cord injury. Brain : a journal of neurology *139*, 1394-1416.
Basak, O., Beumer, J., Wiebrands, K., Seno, H., van Oudenaarden, A., and Clevers, H. (2017). Induced Quiescence of Lgr5+ Stem Cells in Intestinal Organoids Enables Differentiation of Hormone-Producing Enteroendocrine Cells. Cell stem cell *20*, 177-190 e174.
Biteau, B., and Jasper, H. (2011). EGF signaling regulates the proliferation of intestinal stem cells in Drosophila. Development *138*, 1045-1055.
Bolger, A.M., Lohse, M., and Usadel, B. (2014). Trimmomatic: a flexible trimmer for Illumina sequence data. Bioinformatics *30*, 2114-2120.
Britsch, S. (2007). The neuregulin-I/ErbB signaling system in development and disease. Advances in anatomy, embryology, and cell biology *190*, 1-65.
Buchon, N., Broderick, N.A., Kuraishi, T., and Lemaitre, B. (2010). Drosophila EGFR pathway coordinates stem cell proliferation and gut remodeling following infection. BMC biology *8*, 152.
Buczacki, S.J., Zecchini, H.I., Nicholson, A.M., Russell, R., Vermeulen, L., Kemp, R., and Winton, D.J. (2013). Intestinal label-retaining cells are secretory precursors expressing Lgr5. Nature *495*, 65-69.
Burgess, A.W., Cho, H.S., Eigenbrot, C., Ferguson, K.M., Garrett, T.P., Leahy, D.J., Lemmon, M.A., Sliwkowski, M.X., Ward, C.W., and Yokoyama, S. (2003). An open-and-shut case? Recent insights into the activation of EGF/ErbB receptors. Mol Cell *12*, 541-552.
Chiacchiera, F., Rossi, A., Jammula, S., Zanotti, M., and Pasini, D. (2016). PRC2 preserves intestinal progenitors and restricts secretory lineage commitment. The EMBO journal *35*, 2301-2314.
Clevers, H. (2013). The intestinal crypt, a prototype stem cell compartment. Cell *154*, 274-284.
Date, S., and Sato, T. (2015). Mini-gut organoids: reconstitution of the stem cell niche. Annual review of cell and developmental biology *31*, 269-289.
De Schepper, S., Verheijden, S., Aguilera-Lizarraga, J., Viola, M.F., Boesmans, W., Stakenborg, N., Voytyuk, I., Smidt, I., Boeckx, B., Dierckx de Casterle, I.*, et al.* (2018). Self-Maintaining Gut Macrophages Are Essential for Intestinal Homeostasis. Cell *175*, 400-415 e413.
de Sousa, E.M.F., and de Sauvage, F.J. (2019). Cellular Plasticity in Intestinal Homeostasis and Disease. Cell stem cell *24*, 54-64.
Degirmenci, B., Hausmann, G., Valenta, T., and Basler, K. (2018a). Wnt Ligands as a Part of the Stem Cell Niche in the Intestine and the Liver. Progress in molecular biology and translational science *153*, 1-19.
Degirmenci, B., Valenta, T., Dimitrieva, S., Hausmann, G., and Basler, K. (2018b). GLI1-expressing mesenchymal cells form the essential Wnt-secreting niche for colon stem cells. Nature *558*, 449-453.
Dobin, A., Davis, C.A., Schlesinger, F., Drenkow, J., Zaleski, C., Jha, S., Batut, P., Chaisson, M., and Gingeras, T.R. (2013). STAR: ultrafast universal RNA-seq aligner. Bioinformatics *29*, 15-21.
el Marjou, F., Janssen, K.P., Chang, B.H., Li, M., Hindie, V., Chan, L., Louvard, D., Chambon, P., Metzger, D., and Robine, S. (2004). Tissue-specific and inducible Cre-mediated recombination in the gut epithelium. Genesis *39*, 186-193.
Erickson, S.L., O'Shea, K.S., Ghaboosi, N., Loverro, L., Frantz, G., Bauer, M., Lu, L.H., and Moore, M.W. (1997). ErbB3 is required for normal cerebellar and cardiac development: a comparison with ErbB2- and heregulin-deficient mice. Development *124*, 4999-5011.
Farin, H.F., Van Es, J.H., and Clevers, H. (2012). Redundant sources of Wnt regulate intestinal stem cells and promote formation of Paneth cells. Gastroenterology *143*, 1518-1529 e1517.

Farkas, J.E., Freitas, P.D., Bryant, D.M., Whited, J.L., and Monaghan, J.R. (2016). Neuregulin-1 signaling is essential for nerve-dependent axolotl limb regeneration. Development *143*, 2724-2731.
Gemberling, M., Karra, R., Dickson, A.L., and Poss, K.D. (2015). Nrg1 is an injury-induced cardiomyocyte mitogen for the endogenous heart regeneration program in zebrafish. eLife *4*, e05871.
Grant, S., Qiao, L., and Dent, P. (2002). Roles of ERBB family receptor tyrosine kinases, and downstream signaling pathways, in the control of cell growth and survival. Front Biosci *7*, d376-389.
Gregorieff, A., Liu, Y., Inanlou, M.R., Khomchuk, Y., and Wrana, J.L. (2015). Yap-dependent reprogramming of Lgr5(+) stem cells drives intestinal regeneration and cancer. Nature *526*, 715-718.
Greicius, G., Kabiri, Z., Sigmundsson, K., Liang, C., Bunte, R., Singh, M.K., and Virshup, D.M. (2018). PDGFRalpha(+) pericryptal stromal cells are the critical source of Wnts and RSPO3 for murine intestinal stem cells in vivo. Proceedings of the National Academy of Sciences of the United States of America *115*, E3173-E3181.
Harnack, C., Berger, H., Antanaviciute, A., Vidal, R., Sauer, S., Simmons, A., Meyer, T.F., and Sigal, M. (2019). R-spondin 3 promotes stem cell recovery and epithelial regeneration in the colon. Nature communications *10*, 4368.
Horvay, K., and Abud, H.E. (2013). Regulation of intestinal stem cells by Wnt and Notch signalling. Advances in experimental medicine and biology *786*, 175-186.
Horvay, K., Casagranda, F., Gany, A., Hime, G.R., and Abud, H.E. (2011). Wnt signaling regulates Snai1 expression and cellular localization in the mouse intestinal epithelial stem cell niche. Stem cells and development *20*, 737-745.
Horvay, K., Jarde, T., Casagranda, F., Perreau, V.M., Haigh, K., Nefzger, C.M., Akhtar, R., Gridley, T., Berx, G., Haigh, J.J.*, et al.* (2015). Snai1 regulates cell lineage allocation and stem cell maintenance in the mouse intestinal epithelium. The EMBO journal *34*, 1319-1335.
Jarde, T., Evans, R.J., McQuillan, K.L., Parry, L., Feng, G.J., Alvares, B., Clarke, A.R., and Dale, T.C. (2013). In vivo and in vitro models for the therapeutic targeting of Wnt signaling using a Tet-ODeltaN89beta-catenin system. Oncogene *32*, 883-893.
Jarde, T., Kass, L., Staples, M., Lescesen, H., Carne, P., Oliva, K., McMurrick, P.J., and Abud, H.E. (2015). ERBB3 Positively Correlates with Intestinal Stem Cell Markers but Marks a Distinct Non Proliferative Cell Population in Colorectal Cancer. PloS one *10*, e0138336.
Jarde, T., Kerr, G., Akhtar, R., and Abud, H.E. (2018). Modelling Intestinal Carcinogenesis Using In Vitro Organoid Cultures. Methods in molecular biology *1725*, 41-52.
Jarde, T., Lloyd-Lewis, B., Thomas, M., Kendrick, H., Melchor, L., Bougaret, L., Watson, P.D., Ewan, K., Smalley, M.J., and Dale, T.C. (2016). Wnt and Neuregulin1/ErbB signalling extends 3D culture of hormone responsive mammary organoids. Nature communications *7*, 13207.
Jiang, H., Grenley, M.O., Bravo, M.J., Blumhagen, R.Z., and Edgar, B.A. (2011). EGFR/Ras/MAPK signaling mediates adult midgut epithelial homeostasis and regeneration in Drosophila. Cell stem cell *8*, 84-95.
Kabiri, Z., Greicius, G., Madan, B., Biechele, S., Zhong, Z., Zaribafzadeh, H., Edison, Aliyev, J., Wu, Y., Bunte, R.*, et al.* (2014). Stroma provides an intestinal stem cell niche in the absence of epithelial Wnts. Development *141*, 2206-2215.
Kabiri, Z., Greicius, G., Zaribafzadeh, H., Hemmerich, A., Counter, C.M., and Virshup, D.M. (2018). Wnt signaling suppresses MAPK-driven proliferation of intestinal stem cells. The Journal of clinical investigation *128*, 3806-3812.
Koch, S. (2017). Extrinsic control of Wnt signaling in the intestine. Differentiation; research in biological diversity *97*, 1-8.
Lahar, N., Lei, N.Y., Wang, J., Jabaji, Z., Tung, S.C., Joshi, V., Lewis, M., Stelzner, M., Martin, M.G., and Dunn, J.C. (2011). Intestinal subepithelial myofibroblasts support in vitro and in vivo growth of human small intestinal epithelium. PloS one *6*, e26898.

Lee, D., Yu, M., Lee, E., Kim, H., Yang, Y., Kim, K., Pannicia, C., Kurie, J.M., and Threadgill, D.W. (2009). Tumor-specific apoptosis caused by deletion of the ERBB3 pseudo-kinase in mouse intestinal epithelium. The Journal of clinical investigation *119*, 2702-2713.
Lee, K.F., Simon, H., Chen, H., Bates, B., Hung, M.C., and Hauser, C. (1995). Requirement for neuregulin receptor erbB2 in neural and cardiac development. Nature *378*, 394-398.
Lee, K.K., Jo, H.J., Hong, J.P., Lee, S.W., Sohn, J.S., Moon, S.Y., Yang, S.H., Shim, H., Lee, S.H., Ryu, S.H.*, et al.* (2008). Recombinant human epidermal growth factor accelerates recovery of mouse small intestinal mucosa after radiation damage. International journal of radiation oncology, biology, physics *71*, 1230-1235.
Lemmon, M.A., Schlessinger, J., and Ferguson, K.M. (2014). The EGFR family: not so prototypical receptor tyrosine kinases. Cold Spring Harbor perspectives in biology *6*, a020768.
Liao, Y., Smyth, G.K., and Shi, W. (2014). featureCounts: an efficient general purpose program for assigning sequence reads to genomic features. Bioinformatics *30*, 923-930.
Liu, R., Holik, A.Z., Su, S., Jansz, N., Chen, K., Leong, H.S., Blewitt, M.E., Asselin-Labat, M.L., Smyth, G.K., and Ritchie, M.E. (2015). Why weight? Modelling sample and observational level variability improves power in RNA-seq analyses. Nucleic acids research *43*, e97.
Luetteke, N.C., Qiu, T.H., Fenton, S.E., Troyer, K.L., Riedel, R.F., Chang, A., and Lee, D.C. (1999). Targeted inactivation of the EGF and amphiregulin genes reveals distinct roles for EGF receptor ligands in mouse mammary gland development. Development *126*, 2739-2750.
Madisen, L., Zwingman, T.A., Sunkin, S.M., Oh, S.W., Zariwala, H.A., Gu, H., Ng, L.L., Palmiter, R.D., Hawrylycz, M.J., Jones, A.R.*, et al.* (2010). A robust and high-throughput Cre reporting and characterization system for the whole mouse brain. Nat Neurosci *13*, 133-140.
Mah, A.T., Yan, K.S., and Kuo, C.J. (2016). Wnt pathway regulation of intestinal stem cells. The Journal of physiology *594*, 4837-4847.
McCarthy, N., Manieri, E., Storm, E.E., Saadatpour, A., Luoma, A.M., Kapoor, V.N., Madha, S., Gaynor, L.T., Cox, C., Keerthivasan, S.*, et al.* (2020). Distinct Mesenchymal Cell Populations Generate the Essential BMP Signaling Gradient. Cell stem cell *26*, 1-12.
Metcalfe, C., Kljavin, N.M., Ybarra, R., and de Sauvage, F.J. (2014). Lgr5+ stem cells are indispensable for radiation-induced intestinal regeneration. Cell stem cell *14*, 149-159.
Miettinen, P.J., Berger, J.E., Meneses, J., Phung, Y., Pedersen, R.A., Werb, Z., and Derynck, R. (1995). Epithelial immaturity and multiorgan failure in mice lacking epidermal growth factor receptor. Nature *376*, 337-341.
Mihaylova, M.M., Cheng, C.W., Cao, A.Q., Tripathi, S., Mana, M.D., Bauer-Rowe, K.E., Abu-Remaileh, M., Clavain, L., Erdemir, A., Lewis, C.A.*, et al.* (2018). Fasting Activates Fatty Acid Oxidation to Enhance Intestinal Stem Cell Function during Homeostasis and Aging. Cell stem cell *22*, 769-778 e764.
Mileto, S.J., Jarde, T., Childress, K.O., Jensen, J.L., Rogers, A.P., Kerr, G., Hutton, M.L., Sheedlo, M.J., Bloch, S.C., Shupe, J.A.*, et al.* (2020). Clostridioides difficile infection damages colonic stem cells via TcdB, impairing epithelial repair and recovery from disease. Proceedings of the National Academy of Sciences of the United States of America *117*, 8064-8073.
Munoz, J., Stange, D.E., Schepers, A.G., van de Wetering, M., Koo, B.K., Itzkovitz, S., Volckmann, R., Kung, K.S., Koster, J., Radulescu, S.*, et al.* (2012). The Lgr5 intestinal stem cell signature: robust expression of proposed quiescent '+4' cell markers. The EMBO journal *31*, 3079-3091.
Murata, K., Jadhav, U., Madha, S., Van Es, J.H., Dean, J., Cavazza, A., Wucherpfennig, K., Michor, F., Clevers, H., and Shivdasani, R.A. (2020). Ascl2-Dependent Cell Dedifferentiation Drives Regeneration of Ablated Intestinal Stem Cells. Cell stem cell *26*, 377-390.
Nefzger, C.M., Jarde, T., Rossello, F.J., Horvay, K., Knaupp, A.S., Powell, D.R., Chen, J., Abud, H.E., and Polo, J.M. (2016). A Versatile Strategy for Isolating a Highly Enriched Population of Intestinal Stem Cells. Stem cell reports *6*, 321-329.

Nusse, Y.M., Savage, A.K., Marangoni, P., Rosendahl-Huber, A.K.M., Landman, T.A., de Sauvage, F.J., Locksley, R.M., and Klein, O.D. (2018). Parasitic helminths induce fetal-like reversion in the intestinal stem cell niche. Nature *559*, 109-113.
Olayioye, M.A. (2001). Update on HER-2 as a target for cancer therapy: intracellular signaling pathways of ErbB2/HER-2 and family members. Breast Cancer Res *3*, 385-389.
Pejchal, J., Sinkorova, Z., Tichy, A., Kmochova, A., Durisova, K., Kubelkova, K., Pohanka, M., Bures, J., Tacheci, I., Kuca, K.*, et al.* (2015). Attenuation of radiation-induced gastrointestinal damage by epidermal growth factor and bone marrow transplantation in mice. International journal of radiation biology *91*, 703-714.
Phipson, B., Lee, S., Majewski, I.J., Alexander, W.S., and Smyth, G.K. (2016). Robust Hyperparameter Estimation Protects against Hypervariable Genes and Improves Power to Detect Differential Expression. Ann Appl Stat *10*, 946-963.
Potten, C.S., and Grant, H.K. (1998). The relationship between ionizing radiation-induced apoptosis and stem cells in the small and large intestine. British journal of cancer *78*, 993-1003.
Ritchie, M.E., Phipson, B., Wu, D., Hu, Y., Law, C.W., Shi, W., and Smyth, G.K. (2015). limma powers differential expression analyses for RNA-sequencing and microarray studies. Nucleic acids research *43*, e47.
Robinson, M.D., and Oshlack, A. (2010). A scaling normalization method for differential expression analysis of RNA-seq data. Genome Biol *11*, R25.
Rupert, C.E., and Coulombe, K.L. (2015). The roles of neuregulin-1 in cardiac development, homeostasis, and disease. Biomarker insights *10*, 1-9.
Ruzankina, Y., Pinzon-Guzman, C., Asare, A., Ong, T., Pontano, L., Cotsarelis, G., Zediak, V.P., Velez, M., Bhandoola, A., and Brown, E.J. (2007). Deletion of the developmentally essential gene ATR in adult mice leads to age-related phenotypes and stem cell loss. Cell stem cell *1*, 113-126.
Sato, T., van Es, J.H., Snippert, H.J., Stange, D.E., Vries, R.G., van den Born, M., Barker, N., Shroyer, N.F., van de Wetering, M., and Clevers, H. (2011). Paneth cells constitute the niche for Lgr5 stem cells in intestinal crypts. Nature *469*, 415-418.
Sato, T., Vries, R.G., Snippert, H.J., van de Wetering, M., Barker, N., Stange, D.E., van Es, J.H., Abo, A., Kujala, P., Peters, P.J.*, et al.* (2009). Single Lgr5 stem cells build crypt-villus structures in vitro without a mesenchymal niche. Nature *459*, 262-265.
Schindelin, J., Arganda-Carreras, I., Frise, E., Kaynig, V., Longair, M., Pietzsch, T., Preibisch, S., Rueden, C., Saalfeld, S., Schmid, B.*, et al.* (2012). Fiji: an open-source platform for biological-image analysis. Nature methods *9*, 676-682.
Schlessinger, J. (2002). Ligand-induced, receptor-mediated dimerization and activation of EGF receptor. Cell *110*, 669-672.
Sehgal, A., Donaldson, D.S., Pridans, C., Sauter, K.A., Hume, D.A., and Mabbott, N.A. (2018). The role of CSF1R-dependent macrophages in control of the intestinal stem-cell niche. Nature communications *9*, 1272.
Serra, D., Mayr, U., Boni, A., Lukonin, I., Rempfler, M., Challet Meylan, L., Stadler, M.B., Strnad, P., Papasaikas, P., Vischi, D.*, et al.* (2019). Self-organization and symmetry breaking in intestinal organoid development. Nature *569*, 66-72.
Shoshkes-Carmel, M., Wang, Y.J., Wangensteen, K.J., Toth, B., Kondo, A., Massasa, E.E., Itzkovitz, S., and Kaestner, K.H. (2018). Subepithelial telocytes are an important source of Wnts that supports intestinal crypts. Nature *557*, 242-246.
Sibilia, M., and Wagner, E.F. (1995). Strain-dependent epithelial defects in mice lacking the EGF receptor. Science *269*, 234-238.
Srivatsa, S., Paul, M.C., Cardone, C., Holcmann, M., Amberg, N., Pathria, P., Diamanti, M.A., Linder, M., Timelthaler, G., Dienes, H.P.*, et al.* (2017). EGFR in Tumor-Associated Myeloid Cells Promotes Development of Colorectal Cancer in Mice and Associates With Outcomes of Patients. Gastroenterology *153*, 178-190 e110.

Stzepourginski, I., Nigro, G., Jacob, J.M., Dulauroy, S., Sansonetti, P.J., Eberl, G., and Peduto, L. (2017). CD34+ mesenchymal cells are a major component of the intestinal stem cells niche at homeostasis and after injury. Proceedings of the National Academy of Sciences of the United States of America *114*, E506-E513.
Taniguchi, K., Wu, L.W., Grivennikov, S.I., de Jong, P.R., Lian, I., Yu, F.X., Wang, K., Ho, S.B., Boland, B.S., Chang, J.T.*, et al.* (2015). A gp130-Src-YAP module links inflammation to epithelial regeneration. Nature *519*, 57-62.
Tetteh, P.W., Basak, O., Farin, H.F., Wiebrands, K., Kretzschmar, K., Begthel, H., van den Born, M., Korving, J., de Sauvage, F., van Es, J.H.*, et al.* (2016). Replacement of Lost Lgr5-Positive Stem Cells through Plasticity of Their Enterocyte-Lineage Daughters. Cell stem cell *18*, 203-213.
Threadgill, D.W., Dlugosz, A.A., Hansen, L.A., Tennenbaum, T., Lichti, U., Yee, D., LaMantia, C., Mourton, T., Herrup, K., Harris, R.C.*, et al.* (1995). Targeted disruption of mouse EGF receptor: effect of genetic background on mutant phenotype. Science *269*, 230-234.
Tian, H., Biehs, B., Chiu, C., Siebel, C.W., Wu, Y., Costa, M., de Sauvage, F.J., and Klein, O.D. (2015). Opposing activities of Notch and Wnt signaling regulate intestinal stem cells and gut homeostasis. Cell reports *11*, 33-42.
Tian, H., Biehs, B., Warming, S., Leong, K.G., Rangell, L., Klein, O.D., and de Sauvage, F.J. (2011). A reserve stem cell population in small intestine renders Lgr5-positive cells dispensable. Nature *478*, 255-259.
Tripathi, S., Pohl, M.O., Zhou, Y., Rodriguez-Frandsen, A., Wang, G., Stein, D.A., Moulton, H.M., DeJesus, P., Che, J., Mulder, L.C.*, et al.* (2015). Meta- and Orthogonal Integration of Influenza "OMICs" Data Defines a Role for UBR4 in Virus Budding. Cell Host Microbe *18*, 723-735.
Valenta, T., Degirmenci, B., Moor, A.E., Herr, P., Zimmerli, D., Moor, M.B., Hausmann, G., Cantu, C., Aguet, M., and Basler, K. (2016). Wnt Ligands Secreted by Subepithelial Mesenchymal Cells Are Essential for the Survival of Intestinal Stem Cells and Gut Homeostasis. Cell reports *15*, 911-918.
van Es, J.H., Sato, T., van de Wetering, M., Lyubimova, A., Yee Nee, A.N., Gregorieff, A., Sasaki, N., Zeinstra, L., van den Born, M., Korving, J.*, et al.* (2012). Dll1+ secretory progenitor cells revert to stem cells upon crypt damage. Nature cell biology *14*, 1099-1104.
Wang, Y., Chiang, I.L., Ohara, T.E., Fujii, S., Cheng, J., Muegge, B.D., Ver Heul, A., Han, N.D., Lu, Q., Xiong, S.*, et al.* (2019). Long-Term Culture Captures Injury-Repair Cycles of Colonic Stem Cells. Cell *179*, 1144-1159 e1115.
Yui, S., Azzolin, L., Maimets, M., Pedersen, M.T., Fordham, R.P., Hansen, S.L., Larsen, H.L., Guiu, J., Alves, M.R.P., Rundsten, C.F.*, et al.* (2018). YAP/TAZ-Dependent Reprogramming of Colonic Epithelium Links ECM Remodeling to Tissue Regeneration. Cell stem cell *22*, 35-49 e37.
Zhang, J., Eto, K., Honmyou, A., Nakao, K., Kiyonari, H., and Abe, S. (2011). Neuregulins are essential for spermatogonial proliferation and meiotic initiation in neonatal mouse testis. Development *138*, 3159-3168.

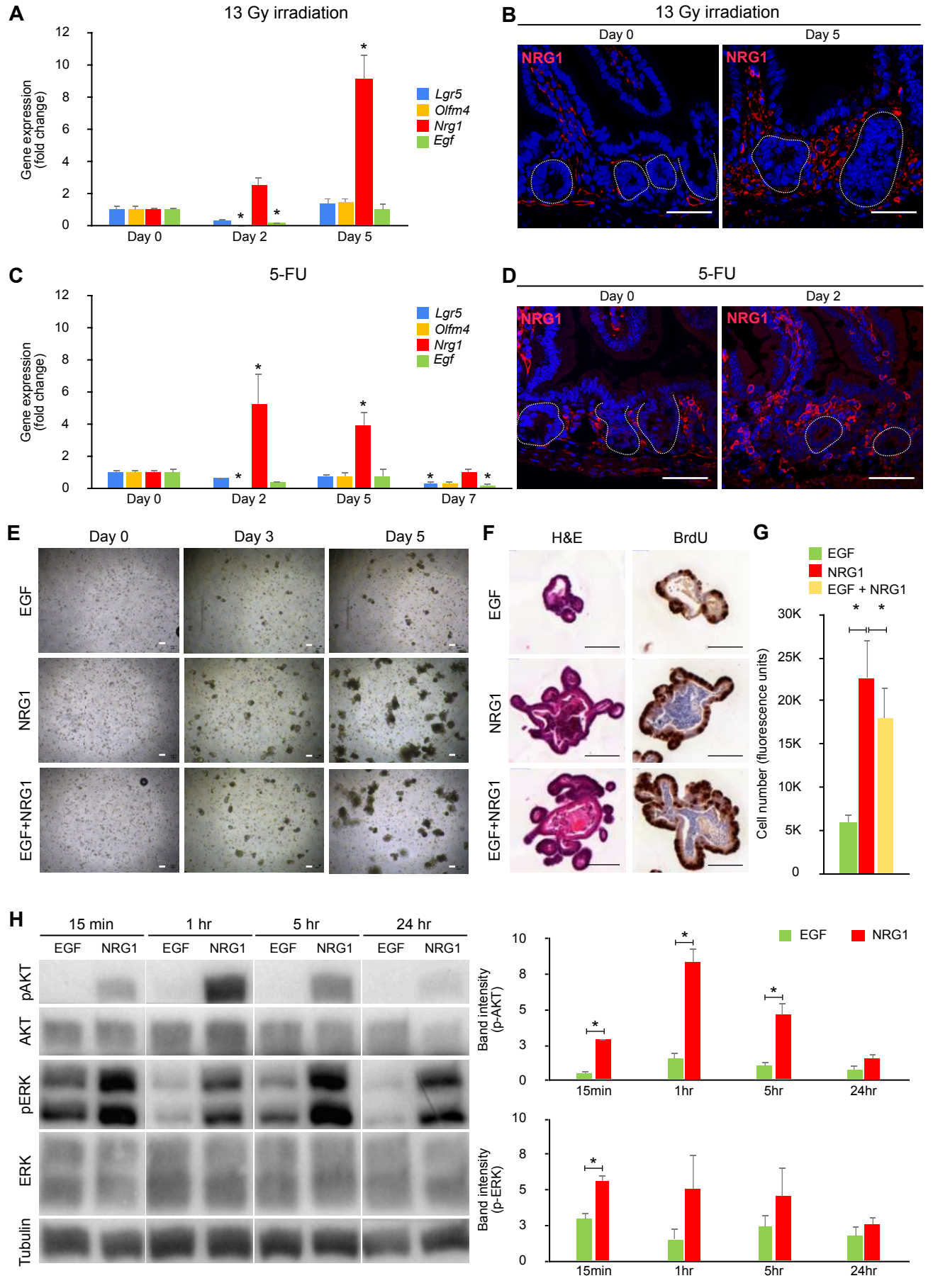
A
13 Gy irradiation
Gene expression (fold change)
Lgr5
Olfm4
Nrg1
Egf
Day 0
Day 2
Day 5
B
13 Gy irradiation
Day 0
Day 5
NRG1
C
5-FU
Day 7
D
5-FU
Day 2
E
Day 3
EGF
NRG1
EGF+NRG1
F
H&E
BrdU
G
EGF + NRG1
Cell number (fluorescence units)
H
15 min
1 hr
5 hr
24 hr
pAKT
AKT
pERK
ERK
Tubulin
Band intensity (p-AKT)
Band intensity (p-ERK)
15min
1hr
5hr
24hr

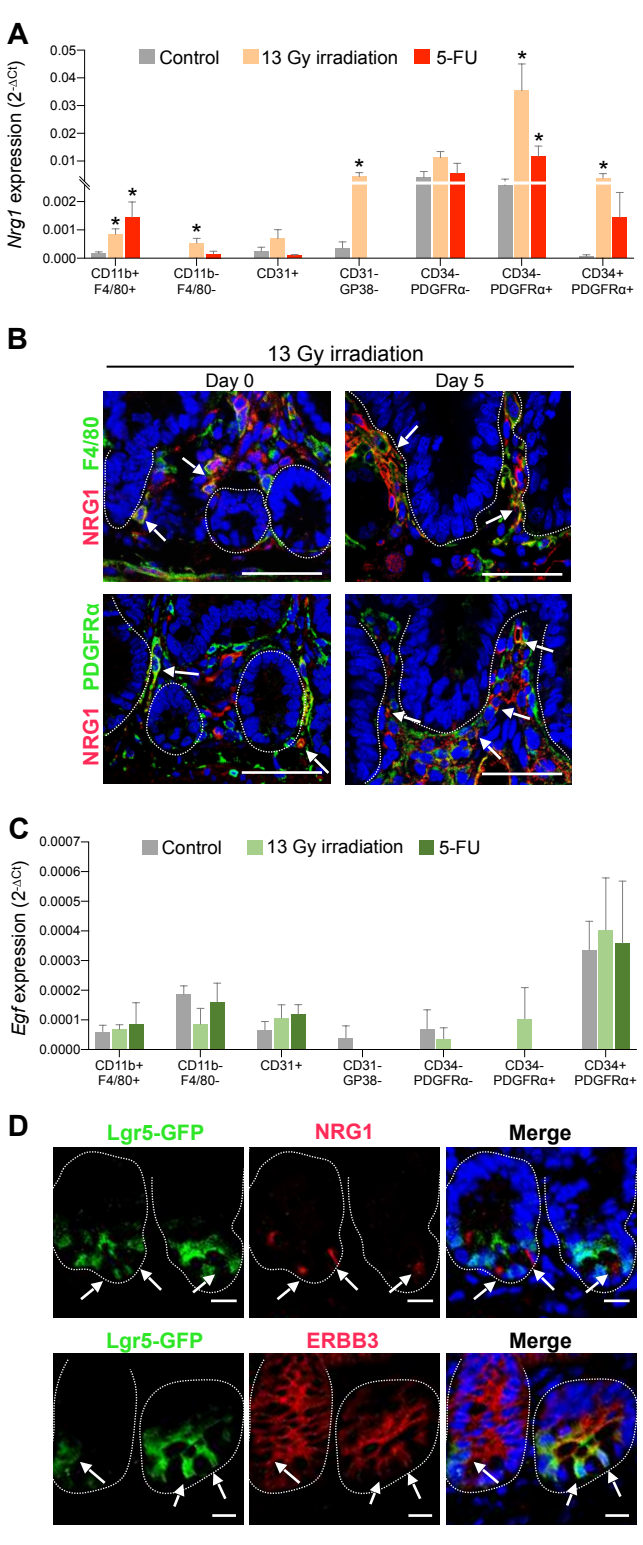
A
Control
13 Gy irradiation
5-FU
Nrg1 expression (2-ΔCt)
0.05
0.04
0.03
0.02
0.01
0.002
0.001
0.000
CD11b+ F4/80+
CD11b- F4/80-
CD31+
CD31- GP38-
CD34- PDGFRα-
CD34- PDGFRα+
CD34+ PDGFRα+
B
13 Gy irradiation
Day 0
Day 5
F4/80
NRG1
PDGFRα
NRG1
C
Control
13 Gy irradiation
5-FU
Egf expression (2-ΔCt)
0.0007
0.0006
0.0005
0.0004
0.0003
0.0002
0.0001
0.0000
CD11b+ F4/80+
CD11b- F4/80-
CD31+
CD31- GP38-
CD34- PDGFRα-
CD34- PDGFRα+
CD34+ PDGFRα+
D
Lgr5-GFP
NRG1
Merge
Lgr5-GFP
ERBB3
Merge

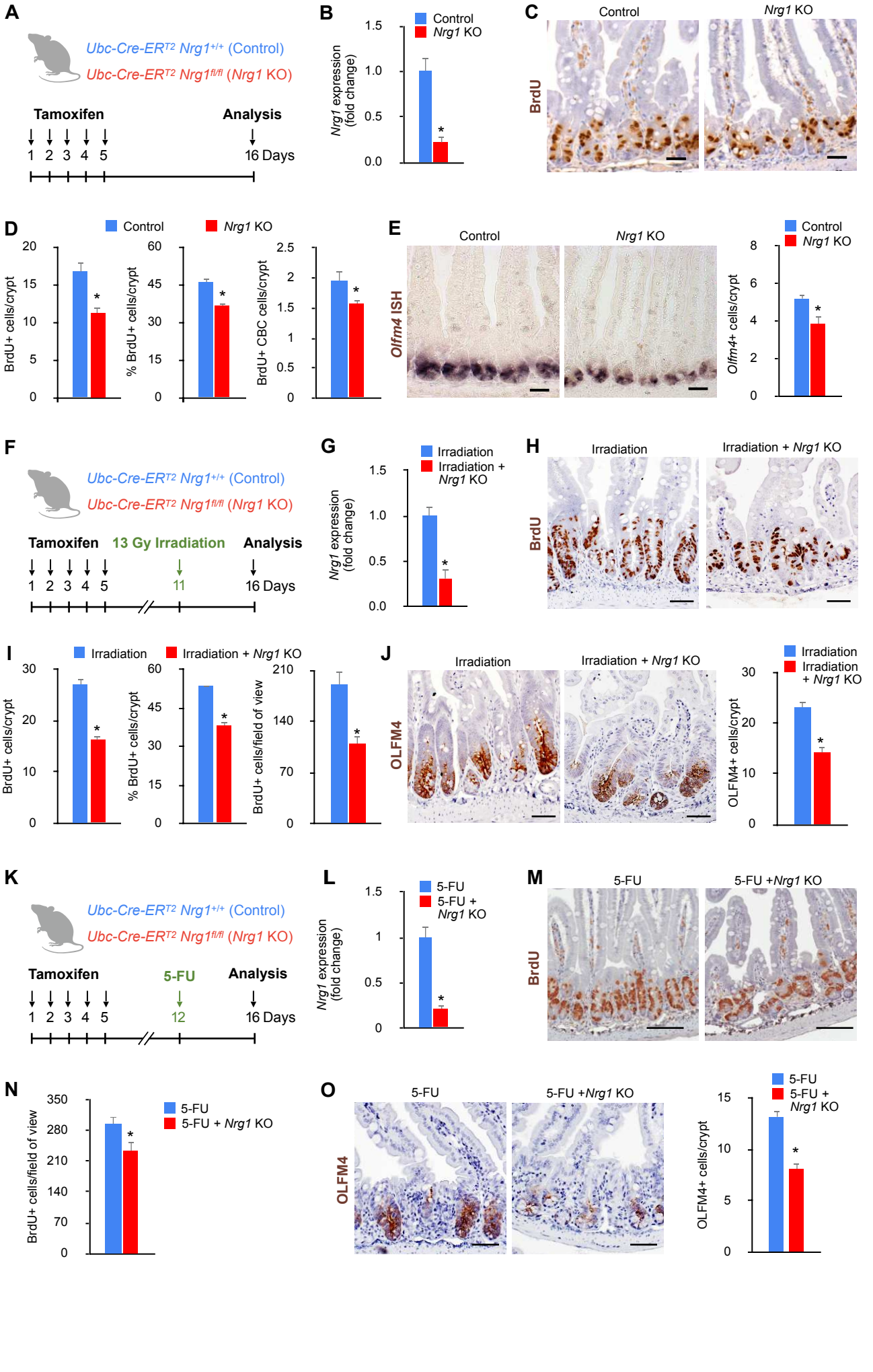
A
Ubc-Cre-ER^{T2} Nrg1$^{+/+}$ (Control)
Ubc-Cre-ER^{T2} Nrg1$^{fl/fl}$ (Nrg1 KO)
Tamoxifen
Analysis
1 2 3 4 5
16 Days
B
Control
Nrg1 KO
Nrg1 expression (fold change)
1.5
1.0
0.5
0.0
*
C
Control
Nrg1 KO
BrdU
D
Control
Nrg1 KO
BrdU+ cells/crypt
% BrdU+ cells/crypt
BrdU+ CBC cells/crypt
E
Control
Nrg1 KO
Olfm4 ISH
Olfm4+ cells/crypt
F
Ubc-Cre-ER^{T2} Nrg1$^{+/+}$ (Control)
Ubc-Cre-ER^{T2} Nrg1$^{fl/fl}$ (Nrg1 KO)
Tamoxifen
13 Gy Irradiation
Analysis
1 2 3 4 5
11
16 Days
G
Irradiation
Irradiation + Nrg1 KO
Nrg1 expression (fold change)
H
Irradiation
Irradiation + Nrg1 KO
BrdU
I
Irradiation
Irradiation + Nrg1 KO
BrdU+ cells/crypt
% BrdU+ cells/crypt
BrdU+ cells/field of view
J
Irradiation
Irradiation + Nrg1 KO
OLFM4
OLFM4+ cells/crypt
K
Ubc-Cre-ER^{T2} Nrg1$^{+/+}$ (Control)
Ubc-Cre-ER^{T2} Nrg1$^{fl/fl}$ (Nrg1 KO)
Tamoxifen
5-FU
Analysis
1 2 3 4 5
12
16 Days
L
5-FU
5-FU + Nrg1 KO
Nrg1 expression (fold change)
M
5-FU
5-FU +Nrg1 KO
BrdU
N
5-FU
5-FU + Nrg1 KO
BrdU+ cells/field of view
O
5-FU
5-FU +Nrg1 KO
OLFM4
OLFM4+ cells/crypt

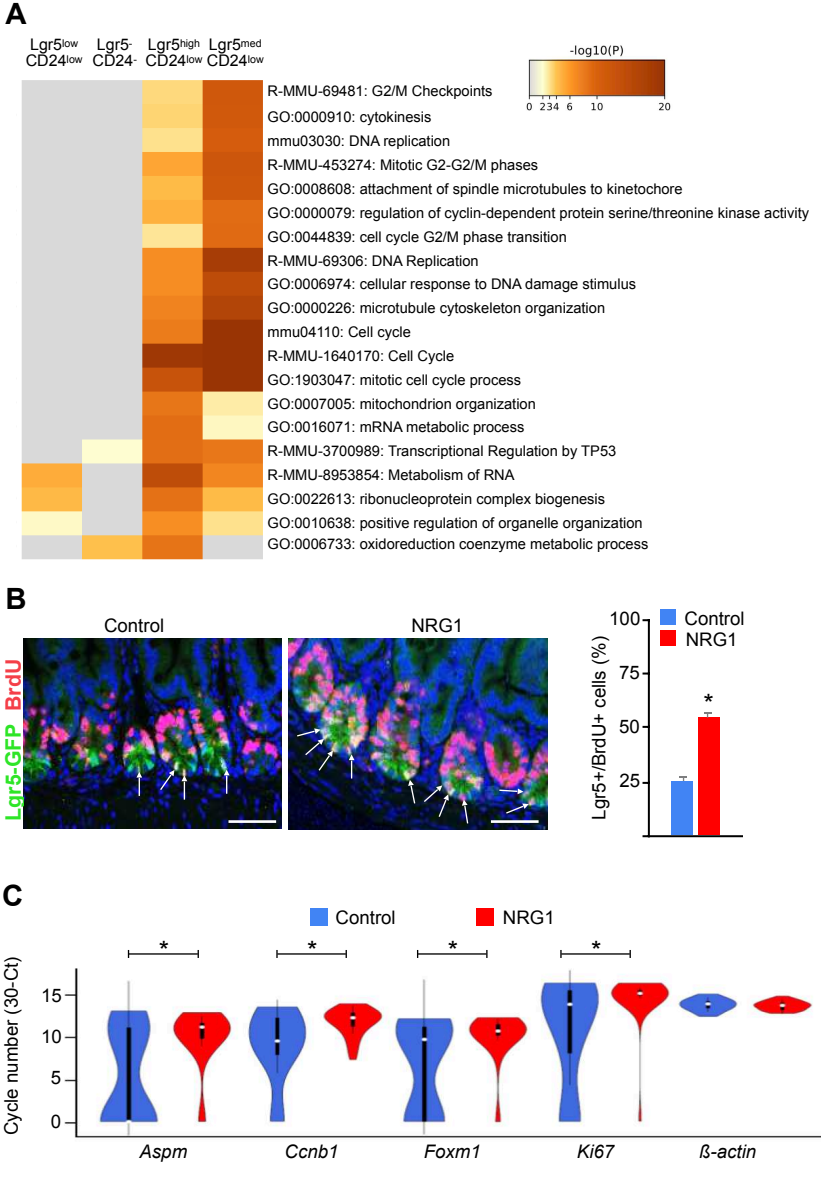
A
Lgr5low CD24low
Lgr5- CD24-
Lgr5high CD24low
Lgr5med CD24low
-log10(P)
0 2 3 4 6 10 20
R-MMU-69481: G2/M Checkpoints
GO:0000910: cytokinesis
mmu03030: DNA replication
R-MMU-453274: Mitotic G2-G2/M phases
GO:0008608: attachment of spindle microtubules to kinetochore
GO:0000079: regulation of cyclin-dependent protein serine/threonine kinase activity
GO:0044839: cell cycle G2/M phase transition
R-MMU-69306: DNA Replication
GO:0006974: cellular response to DNA damage stimulus
GO:0000226: microtubule cytoskeleton organization
mmu04110: Cell cycle
R-MMU-1640170: Cell Cycle
GO:1903047: mitotic cell cycle process
GO:0007005: mitochondrion organization
GO:0016071: mRNA metabolic process
R-MMU-3700989: Transcriptional Regulation by TP53
R-MMU-8953854: Metabolism of RNA
GO:0022613: ribonucleoprotein complex biogenesis
GO:0010638: positive regulation of organelle organization
GO:0006733: oxidoreduction coenzyme metabolic process
B
Control
NRG1
Lgr5-GFP
BrdU
Lgr5+/BrdU+ cells (%)
100
75
50
25
Control
NRG1
*
C
Control
NRG1
Cycle number (30-Ct)
15
10
5
0
*
*
*
*
Aspm
Ccnb1
Foxm1
Ki67
ß-actin

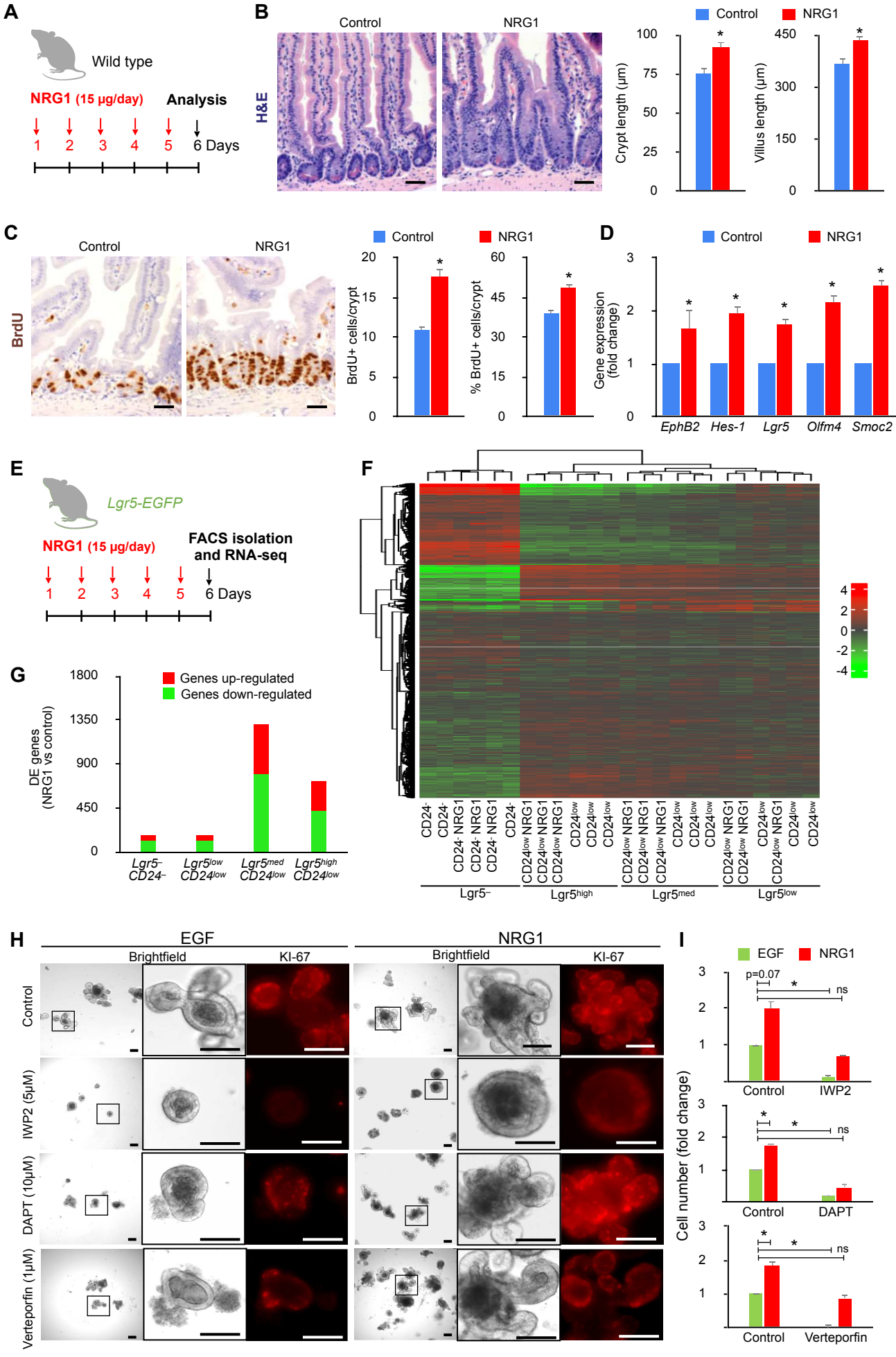
A
Wild type
NRG1 (15 µg/day)
Analysis
1 2 3 4 5 6 Days
B
Control
NRG1
H&E
Crypt length (µm)
Villus length (µm)
C
Control
NRG1
BrdU
BrdU+ cells/crypt
% BrdU+ cells/crypt
D
Gene expression (fold change)
EphB2
Hes-1
Lgr5
Olfm4
Smoc2
E
Lgr5-EGFP
NRG1 (15 µg/day)
FACS isolation and RNA-seq
1 2 3 4 5 6 Days
F
CD24-
CD24- NRG1
CD24low
CD24low NRG1
Lgr5−
Lgr5high
Lgr5med
Lgr5low
G
Genes up-regulated
Genes down-regulated
DE genes (NRG1 vs control)
Lgr5− CD24−
Lgr5low CD24low
Lgr5med CD24low
Lgr5high CD24low
H
EGF
NRG1
Brightfield
KI-67
Control
IWP2 (5µM)
DAPT (10µM)
Verteporfin (1µM)
I
EGF
NRG1
p=0.07
ns
Cell number (fold change)
Control
IWP2
DAPT
Verteporfin

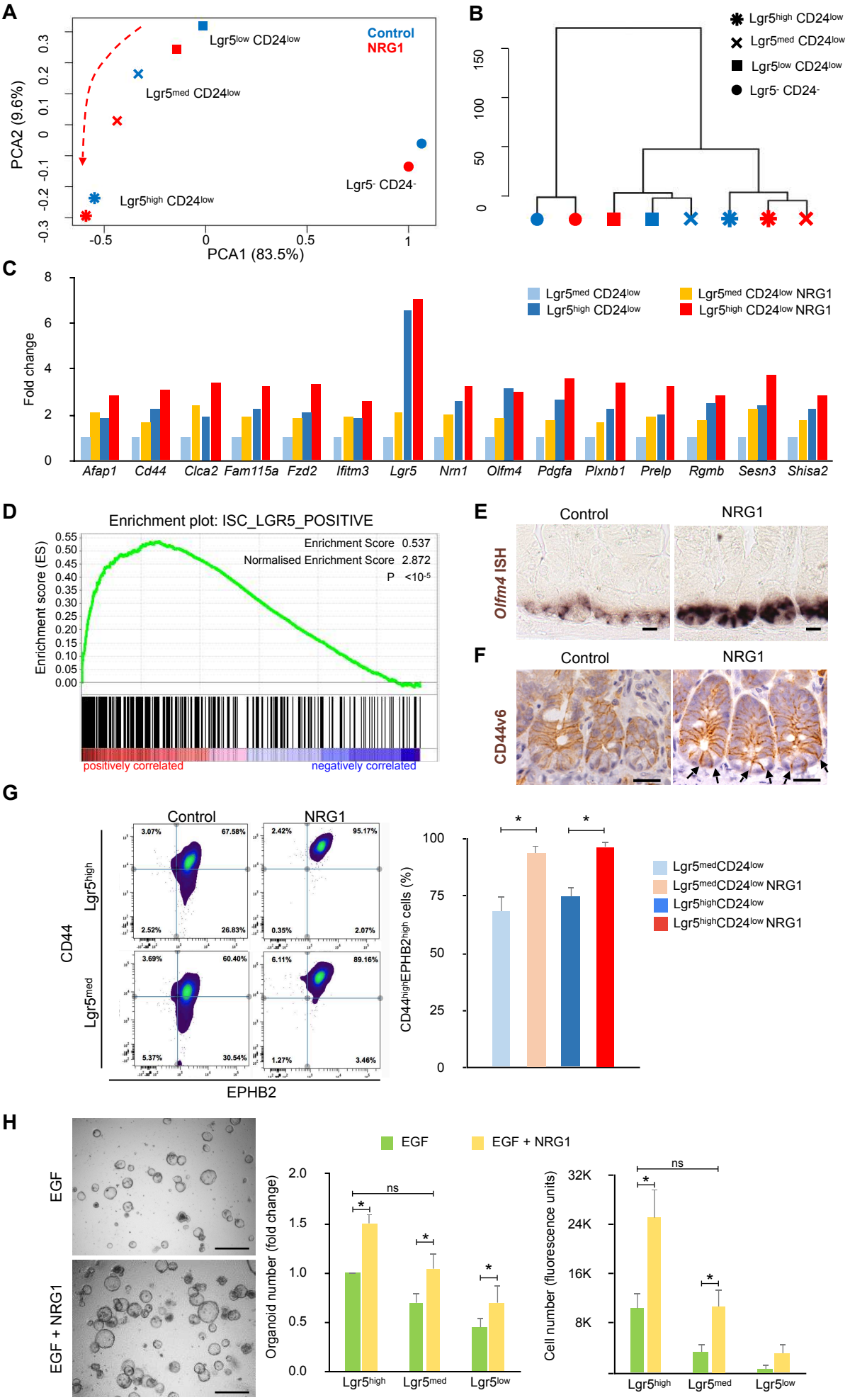
A
Control
NRG1
Lgr5low CD24low
Lgr5med CD24low
Lgr5high CD24low
Lgr5- CD24-
PCA2 (9.6%)
PCA1 (83.5%)
B
Lgr5high CD24low
Lgr5med CD24low
Lgr5low CD24low
Lgr5- CD24-
C
Lgr5med CD24low
Lgr5high CD24low
Lgr5med CD24low NRG1
Lgr5high CD24low NRG1
Fold change
Afap1 Cd44 Clca2 Fam115a Fzd2 Ifitm3 Lgr5 Nrn1 Olfm4 Pdgfa Plxnb1 Prelp Rgmb Sesn3 Shisa2
D
Enrichment plot: ISC_LGR5_POSITIVE
Enrichment Score 0.537
Normalised Enrichment Score 2.872
P <10-5
Enrichment score (ES)
positively correlated
negatively correlated
E
Control
NRG1
Olfm4 ISH
F
Control
NRG1
CD44v6
G
Control
NRG1
Lgr5high
Lgr5med
CD44
EPHB2
3.07%
67.58%
2.52%
26.83%
2.42%
95.17%
0.35%
2.07%
3.69%
60.40%
5.37%
30.54%
6.11%
89.16%
1.27%
3.46%
CD44highEPHB2high cells (%)
Lgr5medCD24low
Lgr5medCD24low NRG1
Lgr5highCD24low
Lgr5highCD24low NRG1
H
EGF
EGF + NRG1
EGF
EGF + NRG1
Organoid number (fold change)
Cell number (fluorescence units)
ns
Lgr5high
Lgr5med
Lgr5low

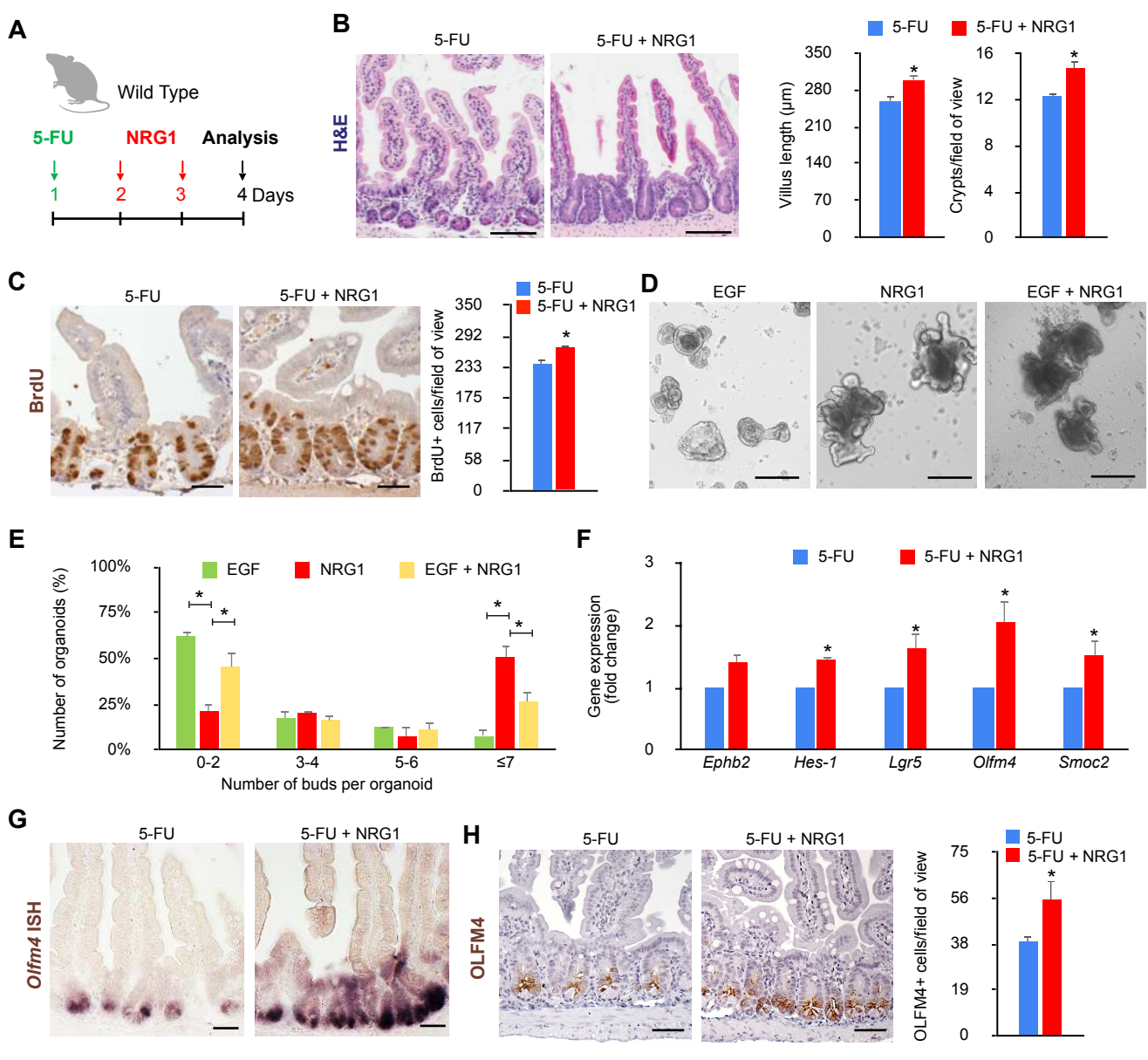
A
Wild Type
5-FU
NRG1
Analysis
1
2
3
4 Days
B
5-FU
5-FU + NRG1
H&E
Villus length (μm)
Crypts/field of view
C
BrdU
BrdU+ cells/field of view
D
EGF
NRG1
EGF + NRG1
E
Number of organoids (%)
Number of buds per organoid
0-2
3-4
5-6
≤7
F
Gene expression (fold change)
Ephb2
Hes-1
Lgr5
Olfm4
Smoc2
G
Olfm4 ISH
H
OLFM4
OLFM4+ cells/field of view